

**Pool Boiling of FC 770 on Graphene Oxide Coatings: A  
Study of Critical Heat Flux and Boiling Heat Transfer  
Enhancement Mechanisms**

Kaushik Sayeemohan

Thesis submitted to the Faculty of the  
Virginia Polytechnic Institute and State University  
in partial fulfillment of the requirements for the degree of

Master of Science  
in  
Mechanical Engineering

Roop L Mahajan, Chair  
Scott T Huxtable  
Srinath Ekkad

June 20, 2016  
Blacksburg, Virginia

**Keywords:** Pool boiling, critical heat flux, graphene oxide, reduced graphene  
oxide, Fluorinert FC 770, Hummer's method

## **Abstract**

Pool Boiling of FC 770 on Graphene Oxide Coatings: A Study of Critical Heat Flux and Boiling Heat Transfer Enhancement Mechanisms

*Kaushik Sayeemohan*

This thesis investigates pool boiling heat transfer from bare and graphene-coated NiCr wires in a saturated liquid of FC 770, a fluorocarbon fluid. Of particular interest was the effect of graphene-oxide platelets, dip-coated onto the heater surface, in enhancing the nucleate boiling heat transfer (BHT) rates and the critical heat flux (CHF) value. In the course of the pool boiling experiment, the primary focus was on the reduction mechanism of graphene oxide. The transition from hydrophilic to hydrophobic behavior of the graphene oxide-coated surface was captured, and the attendant effects on surface wettability, porosity and thermal activity were observed. A parametric sensitivity analysis of these surface factors was performed to understand the CHF and BHT enhancement mechanisms.

In the presence of graphene-oxide coating, the data indicated an increase of 50% in CHF. As the experiment continued, a partial reduction of graphene oxide occurred, accompanied by (a) further enhancement in the CHF to 77% larger compared to the bare wire. It was shown that the reduction of graphene oxide progressively altered the porosity and thermal conductivity of the coating layer

without changing the wettability of FC 770. Further enhancement in CHF was explained in terms of improved porosity and thermal activity that resulted from the partial reduction of graphene-oxide. An implication of these results is that a graphene-oxide coating is potentially a viable option for thermal management of high-power electronics by immersion cooling technology.

## **General Audience Abstract**

Pool Boiling of FC 770 on Graphene Oxide Coatings: A Study of Critical Heat Flux and Boiling Heat Transfer Enhancement Mechanisms

*Kaushik Sayeemohan*

Moore's law states that the number of transistors in an electronic device doubles every year. With a continuing trend in increasing computing abilities, there is an increase in power densities and heat dissipation rates from electronic chips. Heat is an inevitable by-product of power electronics and they have detrimental effects on performance and reliability of the electronic systems. In the present work, an attempt is taken to suggest improvements in direct immersion cooling technology by performing pool boiling experiments. Pool boiling is a phase change process where the heater is immersed in a stagnant pool of saturated liquid. Results show that graphene oxide coating acts as an ideal heater for removing heat effectively even at high heat dissipation densities, and serves as a basis to study the feasibility of applying the current method in thermal management of electronics and super computers.

## **Acknowledgements**

First and foremost, I would like to express the deepest appreciation to my advisor, Dr. Roop L Mahajan, for presenting me with the opportunity to pursue research in this exciting area. I am extremely grateful for his patient guidance and constant encouragement throughout my Master's program. His passion for research, motivation and ideas are contagious, and inspire one and all in ICTAS, and I find myself to be blessed to have the opportunity to work for him during my Master's program at Virginia Tech. Being the Director of ICTAS, despite his heavily packed schedule, Prof. Roop made sufficient time every week to guide me in the right track in my research. Thank you, Dr. Mahajan!

I would like to thank my advisory committee, Drs. Scott Huxtable and Srinath Ekkad for their assistance and constant support. A special thanks to Chris Rowland, my friend, my colleague and my go-to person every time something was wrong, both academically and otherwise. His support, and his ideas have helped me deeply in this work and in my Master's Degree here. I would also like to thank Dr. Karthik Nithyanandam, a mentor, who helped me in understanding the fundamentals of research, and guided me through various challenges I faced as a new graduate student at Virginia Tech. Without his constant encouragement and support, I wouldn't have got the wonderful opportunity to work with Prof. Roop Mahajan.

I would like to express my gratitude to Steve McCartney, of NCFL, for helping me image my graphene oxide samples using scanning electron microscope. I would also like to thank Weinan Leng, of ICTAS I, for helping me with characterizations using Raman spectroscopy and Atomic-force microscopy. .

To my parents, I want to express my deepest gratitude. Words can do little justice to the great deal of sacrifice they have gone through over the two years, just so that I could pursue my dream. I am more the indebted, and in a little big way, blessed! Thank you, Amma and Appa!

# Contents

Abstract.....	ii
General Audience Abstract .....	iv
Acknowledgements .....	v
Contents.....	vii
List of Figures .....	x
List of Tables.....	xiv
1 Introduction .....	1
1.1 Two Phase Heat Transfer: Pool Boiling.....	3
1.2 Graphene: A Potential Heat Transfer Material .....	6
1.3 Review of Boiling Heat Transfer and Critical Heat Flux Enhancements with Graphene Based Materials .....	8
1.4 Layout of the Thesis .....	16
2 Synthesis and Characterization of Graphene Oxide.....	17
2.1 Review of Graphene and nearly Pristine Graphene Synthesis.....	19
2.1.1 Scotch Tape Method: Nobel Prize Winner .....	19
2.1.2 Substrate Based Synthesis .....	20
2.1.3 Solution Based Synthesis .....	21

2.2	Laboratory Synthesis of Graphene Oxide .....	22
2.2.1	Hummer’s Method .....	22
2.2.2	Filtering and Washing of Oxidized Graphite.....	24
2.2.3	Mechanical Exfoliation by Ultra-Sonation .....	24
2.2.4	Coating of Graphene Oxide .....	25
2.3	Characterization of Graphene Oxide .....	29
2.3.1	Raman Spectroscopy.....	30
2.3.2	Scanning Electron Microscopy .....	34
2.3.3	Atomic Force Microscopy .....	37
3	Pool Boiling Experimental Setup and Methods .....	39
3.1	Heater Sample Preparation.....	39
3.2	Resistance –Temperature Characterization for Heating wire .....	40
3.2.1	Experimental Configuration and Method for Temperature-Resistance Calibration.....	40
3.3	Pool Boiling Experimental .....	43
4	Experimental Results and Discussions .....	47
4.1	Hysteresis Analysis.....	47
4.1.1	Critical Heat Flux for Various Heating Surfaces.....	50



4.1.2	Effect of Heater Surface on Hysteresis.....	53
4.2	Analysis of Boiling Curves for Various Heating Surfaces .....	57
4.3	Mechanisms of CHF and BHT Enhancement .....	64
4.3.1	Effect of Wettability .....	65
4.3.2	Effect of Surface Roughness .....	66
4.3.3	Effect of Porosity .....	68
4.3.4	Effect of Thermal Activity .....	74
4.4	Partial Reduction of Graphene Oxide.....	78
5	Conclusion.....	84
	Bibliography .....	87

## List of Figures

Figure 1:1 Pool Boiling: A Representative Sketch.....	4
Figure 1:2 Pool boiling curve showing different regimes of boiling .....	5
Figure 1:3 Allotropes of Sp <sup>2</sup> hybridized carbon atoms: Fullerene, CNTs and Graphene [19], Used under fair use, 2016.....	7
Figure 1:4 CHF Enhancement mechanisms reported for graphene based materials .....	15
Figure 2:1 Dip coating of graphene oxide on NiCr wire: A representative picture	27
Figure 2:2 Spray coating of graphene oxide on flat substrates: A representative picture .....	28
Figure 2:3 Preparation of graphene oxide paper: A representative picture .....	30
Figure 2:4 SP <sup>2</sup> hybridized carbon atoms in a sheet of graphene: A schematic representation.....	31
Figure 2:5 Raman spectrum of graphene oxide paper.....	33
Figure 2:6 SEM Images of graphene oxide layers on NiCr wire at various magnification levels (a) represents uniform coating of dip-deposited GO on NiCr Wire, (b) and (c) shows the self-assembled porous structure and (d) shows the bending of graphene oxide sheet that induces nano- roughness. ....	35

Figure 2:7 SEM Images of graphene oxide paper at various magnification levels. (a) and (b) clearly shows the characteristically ordered porous surface. (c) Shows the layers of graphene oxide stacked on one another. ....36

Figure 2:8 Surface topology of graphene oxide coatings on NiCr wire. The heat map clearly depicts the nano and micro-roughness of porous graphene oxide layer assembled on the surface ..... 37

Figure 3:1 Experimental setup for resistance-temperature characterization of NiCr wire..... 41

Figure 3:2 Resistance-temperature characterization plot for NiCr wire .....42

Figure 3:3 Pool boiling setup.....43

Figure 3:4 Boiling curve for bare NiCr wire in FC-770 until the critical heat flux was reached.....46

Figure 4:1 Visualization of bubbles coalescing just after the CHF point is reached on a bare NiCr wire ..... 51

Figure 4:2 Pool Boiling curves for bare, scratched and graphene oxide coated wires .....53

Figure 4:3 Hysteresis effect observed for FC-77 boiling on bare NiCr wire .....54

Figure 4:4 Heating and cooling curves for FC 770 boiling on scratched wire.....55

Figure 4:5 Heating and cooling curves for FC 770 boiling on graphene oxide-coated wire.....56

Figure 4:6 Boiling curve for bare nichrome wire showing free convection, nucleate boiling and film boiling regime .....	58
Figure 4:7 Visualization of pool boiling of FC 770 on bare NiCr wire in (a) Free convection region, (b) Nucleate boiling region and (c) Film boiling region .....	60
Figure 4:8 Boiling curve for scratched nichrome wire showing free convection, nucleate boiling and film boiling regime .....	60
Figure 4:9 Boiling curve for graphene oxide-coated nichrome wire showing free convection, nucleate boiling and film boiling regime .....	62
Figure 4:10 Visualization of nucleation site density for the same heat flux of 90 kW/m <sup>2</sup> (a) Bare wire and (b) Graphene oxide coated wire. The number of active nucleation site density for graphene oxide coated wire is observed to be significantly higher than that for a bare wire.....	63
Figure 4:11 Apparent contact angle of FC 770 on (a) bare wire, (b) scratched wire and (c) graphene oxide coated wire.....	65
Figure 4:12 Effect of surface roughness on nucleate boiling heat transfer .....	66
Figure 4:13 SEM Image of porous graphene oxide coating on NiCr wire .....	68
Figure 4:14 Photographs taken at 90% of CHF for (a) bare wire and (b) graphene oxide coated wire. The picture clearly depicts the highly populated nucleation sites for a porous graphene oxide layer as compared against a bare NiCr wire.....	70
Figure 4:15 Sensitivity of porosity with predicted CHF (Polezhaev and Kovalev [41]).....	72

Figure 4:16 Sensitivity of permeability with predicted CHF (Liter and Kaviany [42]).....	73
Figure 4:17 CHF as a function of thermal activity of the heating material .....	77
Figure 4:18 Contact angle of water droplet on graphene oxide coated wires at various nucleate boiling dwell times. There is a significant increase in contact angle, showing that the surface is tending towards hydrophobicity, a characteristic property of pristine graphene.....	79
Figure 4:19 Contact angle as a function of nucleate boiling dwell time .....	80
Figure 4:20 Raman spectrum of graphene oxide coating taken at different dwell times. There is a gradual increase in the $I_D/I_G$ intensity ratio, indicating the increase in surface defects. ....	81
Figure 4:21 CHF as a function of nucleate boiling dwell time. There is an increase in CHF with increasing operation time of the heater.. ....	82

## List of Tables

Table 1-1 Review on Critical Heat Flux Enhancement with Graphene Based Materials.....	14
Table 3-1 Heater wire samples for pool boiling experiments .....	39
Table 4-1 Experimental CHF values of bare wire, scratched wire and graphene oxide wire heaters .....	52

# Chapter 1

## 1 Introduction

Several thermal systems involve two phase heat transfer phenomena namely boiling and condensation. A closed loop steam cycle can be considered as an exemplar where pressurized water is converted into vapor in a boiler and is converted back to water using a condenser. Boiling and condensation play an essential role in evaporators and condensers respectively in a vapor compression refrigeration cycle. An attractive characteristic of two phase heat transfer is its extremely high heat transfer coefficient, and hence high heat transfer rates can be achieved even at very low temperature gradients. Researchers and engineers have taken advantage of these heat transfer rates to enhance the performance and safety of moderators in nuclear power plants, and improve thermal management of high power electronic devices.

Following Moore's law, the number of transistors per square inch on integrated circuits has doubled every year since its invention. This has led to a continuing trend in rapid increase in the power densities of electronic devices leading to challenging thermal management problems. For high power electronic devices and super computers, direct liquid immersion two phase cooling has a greater potential when compared to air -cooled technologies because of the high latent heat and heat transfer coefficient involved. There are a number of immersion

cooling technologies adopted for high power super computers, such as Cray-2 cooling system, which involve pool boiling and forced convection boiling of FC 77, a dielectric fluorocarbon fluid. An excellent review of thermal management of advanced computers and electronics has been conducted by Bar-Cohen [1] where prospects for widespread implementation of direct liquid cooling technology in electronics industry are discussed.

In a pool boiling process, critical heat flux (CHF) is the upper limit or the maximum heat transfer rate that occurs by latent heat transfer and/or bubble motion. Hence, the enhancement of CHF is desirable with potential for large impact on many engineering applications such as thermal management of high power density electronics and nuclear plants. Over the decades, there has been an increasing interest in the study of CHF and pool boiling heat transfer (BHT) performance enhancement techniques among researchers.

In boiling heat transfer process, one of the most interesting features of nanoparticles deposition on heat transfer surface, is their capability to enhance the critical heat flux (CHF) [2]. In the past, a substantial amount of research has been conducted to study the pool boiling and flow boiling heat transfer processes using nanofluid, and modified surfaces with micro or nano-structures [3]. Graphene has attracted several researchers because of its extremely good thermal, electrical and mechanical properties. Graphene's thermal conductivity at room temperature is in the range of 3500- 5300 W/m<sup>2</sup> K. Due to its extremely high thermal conductivity,



graphene is a promising material in thermal management applications [4]. Thus, a graphene based material, graphene oxide or chemically converted graphene was chosen for inducing surface modifications and achieve improvements in boiling heat transfer performance. Since the motivation behind the project is thermal management of electronics, we use saturated Fluorinert FC as the working fluid in conducting all the experiments throughout the project. Being a part of fluorocarbons family, FC 770 possesses extremely good dielectric properties, and is chemically inert. A brief revisit to the basics of pool boiling process is provided in section 1.1 to elucidate the experimental methods and discussions reported in the upcoming chapters in this thesis. An introduction to the graphene and a review of boiling heat transfer research conducted using graphene based materials is provided in the sections 1.2 and 1.3, in that order.

## **1.1 Two Phase Heat Transfer: Pool Boiling**

Pool boiling is a process in which the heater surface is immersed in a stagnant liquid body at saturation conditions [5]. It is characterized by evaporation of stationary working fluid at the solid-liquid interface. Evaporation of liquid occurs when the temperature of the surface is greater than the saturation temperature corresponding to that liquid pressure. The heat flux by Newton's law of cooling for this phenomena is given as,

$$q_s'' = h(T_s - T_{sat}) = h(\Delta T_{excess})$$

where  $T_s$  is the surface temperature,  $T_{sat}$  is the saturation temperature of the liquid and  $h$  is the heat transfer coefficient. Pool boiling process involves the formation of vapor bubbles, bubble growth and bubble departure from the surface. The dynamics of bubbles in this process is dependent on the excess temperature, combined properties of the fluid and surface, which in turn affects the heat transfer coefficient.

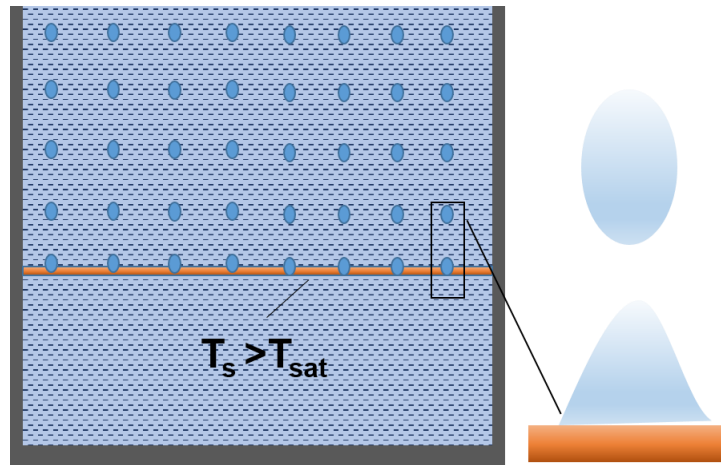


*Figure 1:1 Pool Boiling: A Representative Sketch*

A boiling curve is a graph in which applied heat flux ( $q''$ ) is plotted against the superheat ( $\Delta T_{excess}$ ) experienced by the heating surface. The first pool boiling curve was obtained by Nukiyama in 1934 where he discussed in detail the experimental configuration and regimes of pooling boiling [6]. The different regimes of pool boiling delineated based on the excess temperature were free convection boiling, nucleate boiling, transition boiling and film boiling. To obtain the pool boiling curve, the applied heat flux was gradually increased in steps and

the corresponding wall temperatures were recorded. Excess temperature or wall superheat was defined as the difference between the heater temperature and the saturation temperature of the fluid. Free convection boiling took place when the excess temperature ( $\Delta T_{excess}$ ) was less than the superheat corresponding to the point *B* in Figure 1:2. It was observed that free convection boiling normally occurred below a superheat of  $\sim 5^\circ\text{C}$ , and the motion of the fluid was primarily governed by buoyancy effects. Nucleate boiling occurred between the points *B* and *D* in the boiling curve shown in Figure 1:2. The point *B* was called the onset of nucleate boiling point (ONB), and in the region between *B* and *C*, bubble nucleation occurred at the nucleation sites or boiling centers on the heater surface. Nucleation sites were defined as the spots on the heater surface with characteristic defects or non-homogeneity. The nucleation and departure of bubbles governed the heat transfer coefficient and an increase in bubble nucleation centers increased the slope of the curve. In the region between *C* and *D*, the rate of bubble growth

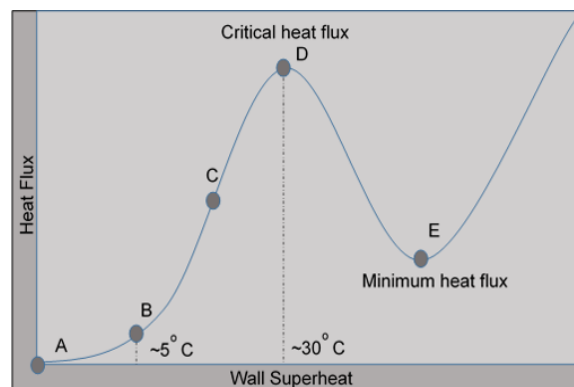


*Figure 1:2 Pool boiling curve showing different regimes of boiling*

further increased and the bubbles departed as columns. This resulted in the coalescence of bubbles, and increased the area of vapor regions near the surface, which in turn reduced the slope of the curve. From point *C* on the graph, the heat flux increased gradually and reached a maximum value termed as critical heat flux (CHF). Transition boiling took place between the points *D* and *E* until an excess temperature of  $\sim 120^{\circ}\text{C}$  was reached. In this region, a blanket of vapor was formed around the surface. Since the thermal conductivity of vapor was very low, the applied heat flux significantly decreased. The point *E* where the minimum heat flux occurred was named as the *Leidenfrost* point. *Leidenfrost* point was defined as the point above which the rewetting of surface by the working fluid was completely inhibited. Beyond the point *D*, heat transfer from the surface was significantly governed by conduction and radiation through the vapor.

Among the four regimes of pool boiling discussed above, nucleate boiling is of primary importance as the heat transfer rate is substantially high even at lower wall superheats. The primary objective of this project is to study the different regimes of boiling for FC 770 for a heater surface coated with graphene oxide and reduced graphene oxide.

## **1.2 Graphene: A Potential Heat Transfer Material**

Graphene is a two-dimensional sheet of  $\text{sp}^2$ -hybridized carbon atoms. A sheet of graphene is a fundamental block to create other allotropes. It can be arranged in stacks to form graphite, rolled to form carbon nano tubes, and wrapped to form

fullerene as depicted in Figure 1:3. The excellent mechanical and thermal properties of graphene come from the long range  $\pi$ -configuration [7]. Graphene has been widely studied for applications in thermal-fluid technologies including heat exchangers, nuclear power plants and electronics thermal management [4]. The thermal conductivity of graphene is much higher than the commonly available conductive materials such as copper with the orders of hundreds of magnitude [8].

The critical heat flux enhancement and improved boiling heat transfer performance can be achieved by carefully controlling the surface roughness, wettability, critical instability wavelength, thermal activity, porosity and capillary wicking action. It has been found that dispersions of graphene platelets in acetone/water mixture at various proportions enable manipulation of surface tension of the nanofluid [9]. The functionalization of surface in terms of roughness

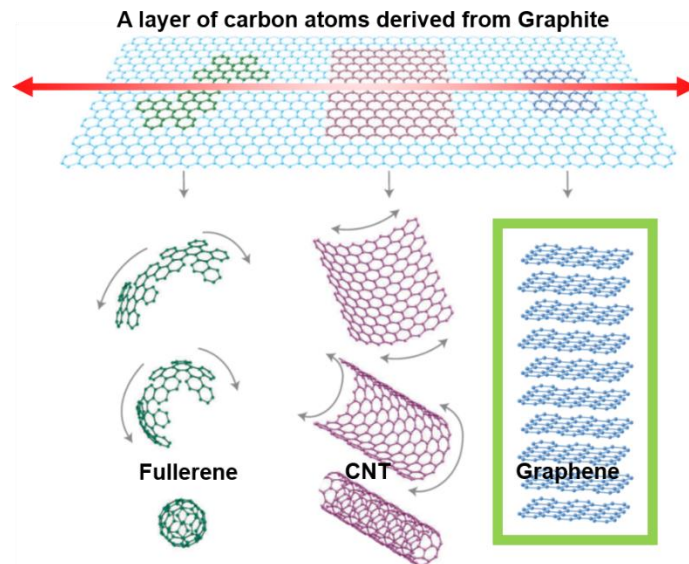


Figure 1:3 Allotropes of  $Sp^2$  hybridized carbon atoms: Fullerene, CNTs and Graphene [19], Used under fair use, 2016

and wettability using graphene coatings can be taken as an advantage in improving the heat dissipation process and reliability of cooling technologies [10]. Hence, graphene can be considered as a potential material for achieving a breakthrough in thermal management techniques.

One of the major challenges faced is formulating a highly scalable and an efficient synthesis method for pristine graphene. In this project, a highly scalable method for a graphene based material called graphene oxide is formulated and processed for studying pool boiling phenomena. Graphene oxide is also a  $sp^2$  configured carbon sheet with functional oxygen, hydroxyl and carboxylic groups, and its reduction process yields completely or partially reduced graphene oxide whose properties are closely aligned with those of a pristine graphene. The graphene based materials focused in this thesis are graphene oxide (GO) and reduced graphene oxide (rGO). The synthesis, properties and the effects of graphene oxide coatings on heater surface are studied in further details in chapters 2 and 4.

### **1.3 Review of Boiling Heat Transfer and Critical Heat Flux Enhancements with Graphene Based Materials**

Park et al. [4] performed pool boiling experiments with a nickel-chromium (80-20) wire in nanofluids containing reduced graphene oxide and graphene oxide nanosheets. They observed an enhancement of about 179% in critical heat flux for a graphene oxide colloidal solution, and 84% for a reduced graphene oxide

nanofluid as compared against the CHF of pure deionized water. They observed that the graphene oxide showed a characteristically ordered porous structure during the pool boiling process. They reported that the CHF enhancements were surprisingly not due to improved surface wettability and capillary action resulting from the porous deposition of graphene oxide layers, but due to the increased thermal activity and critical instability wavelength of graphene oxide layer. They concluded that the reduced graphene oxide and graphene oxide layers on the wires modulated the shorter instability wavelength, which enhanced the CHF.

Park et al. [11] studied the combined effects of highly thermal conductive graphene oxide nanoplatelets and nuclear coolant chemicals on critical heat flux (CHF) limit for potential application in external reactor vessel cooling (ERVC), an accident management strategy in nuclear plants. The pool boiling experiment was carried out on a NiCr wire heater and the effects of wire orientation  $0^\circ < \theta < 90^\circ$  on CHF under various chemical environments were studied. They observed that the graphene oxide nanofluids were stable under the ERVC coolant chemical environments. A maximum CHF enhancement of 40% was achieved at  $90^\circ$  orientation, and 200% for  $0^\circ$  orientation of the wire in comparison to pure water. The CHF enhancement was attributed to the formation of a porous coating on the wire heater surface during the boiling process. The porous structure formation remained unaffected at various chemical environments, and the complex

deposition combined with different chemicals caused variations in CHF enhancements.

Zhang et al. [12] conducted transient quenching experiments to obtain boiling curve for pure water and graphene oxide colloids. They used nickel plated copper spheres as the heater surface. Commercially available concentrated GO dispersions were used and very dilute dispersions were prepared by vigorous sonication. The copper sphere, assumed to be a lumped system was heated to 400°C in a furnace, and quenched in pure water and GO dispersions to obtain transient boiling curves. The critical heat flux of the GO samples were increased by 13.2 % and 25% respectively with increasing concentration. They observed fish-scale shaped graphene oxide nanosheets (GONs) deposited on the surface that were self-assembled during the boiling process. This porous deposition on the heated surface improved the wettability and capillarity of the surface, which enhanced the CHF.

Ahn et al. [13] studied the effect of reduced graphene oxide (rGO) coatings, which contained negatively charged –COOH groups on NiCr wires by conducting Joule heating experiment. They observed a biased coating of rGO at the anode end of the wire because of the electrophoresis phenomena induced by DC power. It was observed that rGO colloid initially increased the CHF by 20%, and a maximum CHF enhancement of 320% was achieved in double side coated wires. The enhancement in CHF was attributed mainly to the increased thermal activity,



porosity of the rGO coating, capillary action that improved wettability and reduced Raleigh-Taylor (RT) wavelength.

Lee et al. [14] enhanced the critical heat flux (CHF) of flow boiling process using graphene oxide colloids at low pressure low flow conditions (LPLF). A maximum CHF enhancement of about 100 % was attained for an inlet temperature of 25° C and mass flux of 250 kg/m<sup>2</sup>s. The maximum CHF observed for 50° C inlet temperature at the same inlet mass flux conditions was about 72%. The enhancement of CHF was caused due to the improved wettability of the inner tube, which resulted from deposition of nanoparticles on the inner surface. The improved wettability made the liquid film more stable and delayed the drying process. This result is in contradiction with the results of Park et al. [4] as the author speculates that GO might have been converted into rGO during pool boiling process rendering the surface less wettable. The author speculates that GO remained unconverted throughout the flow boiling process, and thus the surface wettability had improved.

Ahn et al. [15] reported a novel type of boiling heat transfer that occurred near the critical heat flux region during pool boiling in reduced graphene oxide (rGO) nanofluid. When the CHF point was approached, a gradual rise in the wall temperature for 170 min at a constant heat flux was observed instead of a sudden transition from nucleate boiling to transition boiling with a rapidly increased wall temperature, which could be useful to prevent heater failure during boiling. This

type of behavior was mainly because of the formation of self-assembled porous layer of graphene oxide on the heater surface, which increased the portion of nucleate boiling at the transition boiling regime, preventing the CHF from triggering. They explained that the high thermal activity, which is a function of thermal conductivity and thickness of the deposited layer, was the reason behind the enhancement of CHF.

Kim et al. [16] investigated the boiling heat transfer characteristic for graphene oxide (GO) colloids prepared at various concentration levels. They observed a correlation between concentration of the nanofluid and the thickness of the resulting GO layer on heater surface, which varied the critical heat flux proportionately. Thermal activity, which is proportional to the thermal conductivity and effective thickness of coating, increased with coating thickness, and spread the heat efficiently delaying the occurrence of CHF phenomena. They also found that preheating of GO at 100°C for 12 h partially converted the graphene oxide colloid to form reduced graphene oxide colloid, which further enhanced the CHF.

Park et al. [17] examined the pool boiling characteristics of oxidized multi-walled carbon nanotubes (MWCNT) and oxidized graphene coated surfaces. The colloidal dispersions of as-synthesized carbon based materials were spray-deposited on various heater surfaces with varying deposition times. Their results showed that the contact angle subtended on the surface decreased linearly with an

increase in deposition time. They also observed an increase in critical heat flux (CHF) inversely with the contact angle for both the carbon allotropes. They were able to obtain a maximum CHF enhancement of 63.63% at 0° contact angle for oxidized MWCNT, and a maximum enhancement of 67.27% for oxidized graphene coated surface at 0° contact angle. However, a maximum pool boiling heat transfer coefficient was observed for contact angles of 19.8° and 21.7°, respectively for oxidized MWCNT and oxidized graphene. They attributed the decrease in heat transfer coefficients at very low contact angles to the fouling effect, which occurred due to the reduced bubble generation at the heater surface with increasing heat transfer.

Seo et al. [18] studied the critical heat flux and boiling heat transfer (BHT) enhancement mechanisms for bare indium titanium oxide, porous and non-porous graphene surfaces with the highly wettable FC 72 as the working fluid. The highly conductive non-porous graphene coating enhanced the critical heat flux by 15.7%, and porous graphene coating increased the CHF by 90% when compared against bare heater surface. Since the working fluid used was highly wettable with lower surface tension compared to water, wettability was not considered as one of the factors influencing CHF. They stated that hydrodynamic limit (porosity) and capillary pumping limit (permeability) that resulted from the porous structures were the main factors in addition to high thermal properties of graphene, which caused CHF and BHT enhancements.

Table 1-1 Review on Critical Heat Flux Enhancement with Graphene Based Materials

Literature	Type of Boiling	Working Fluid	Heater Surface	Coating Method	Percentage Enhancement in CHF (%)	Enhancement Mechanism (s)
Park et al [4]	Pool Boiling	<ul style="list-style-type: none"> <li>GO nanofluid</li> <li>rGO nanofluid</li> </ul>	NiCr wire	N/A	<ul style="list-style-type: none"> <li>179 (GO)</li> <li>84 (rGO)</li> </ul>	<ul style="list-style-type: none"> <li>Thermal Activity</li> <li>Critical instability wavelength</li> </ul>
Park et al [11]	Pool Boiling	GO colloids + nuclear coolant chemicals	NiCr wire	N/A	200	<ul style="list-style-type: none"> <li>Self-assembled porous layer</li> </ul>
Zhang et al [12]	Transient Quenching	GO colloids	Ni plated Cu spheres	N/A	25	<ul style="list-style-type: none"> <li>Self-assembled porous layer</li> <li>Wettability</li> <li>Capillarity</li> </ul>
Ahn et al [13]	Pool Boiling	rGO colloids	NiCr wire	N/A	320	<ul style="list-style-type: none"> <li>Thermal activity</li> <li>Porosity</li> <li>Wettability</li> <li>Critical Instability wavelength</li> </ul>
Lee et al [14]	Flow Boiling	GO nanofluids	SS tube	N/A	72	<ul style="list-style-type: none"> <li>Wettability</li> </ul>
Ahn et al [15]	Pool Boiling	rGO colloids	Si plate and Cu cylinder	N/A	80	<ul style="list-style-type: none"> <li>Thermal activity</li> <li>Wettability</li> <li>Capillarity</li> </ul>
Kim et al [16]	Pool Boiling	GO colloids	NiCr wire	N/A	150	<ul style="list-style-type: none"> <li>Thermal Activity</li> </ul>
Park et al [17]	Pool Boiling	Distilled water	Zr flat plate	Spray Coating	62.27	<ul style="list-style-type: none"> <li>Wettability</li> <li>Thermal Activity</li> </ul>
Seo et al [18]	Pool Boiling	FC 72	ITO plate	RTA and nucleate boiling coating	90	<ul style="list-style-type: none"> <li>Porosity</li> </ul>

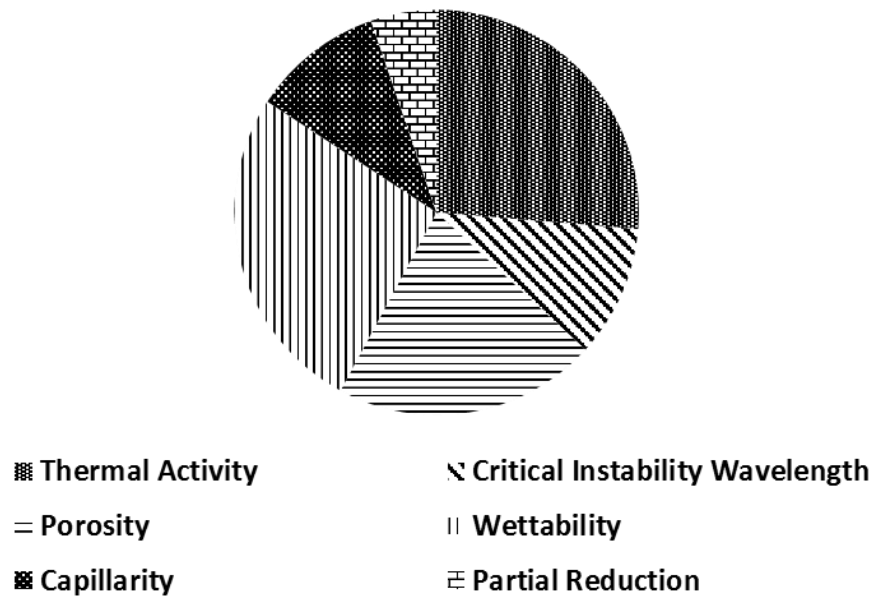


*Figure 1:4 CHF Enhancement mechanisms reported for graphene based materials*

Figure 1:4 reports the CHF enhancement mechanisms for pool boiling experiments conducted using graphene based materials. From the above review of literature, it can be clearly seen that no attempts were made to study the phenomenon of hysteresis and mechanism of reduction of graphene oxide as the pool boiling experiment progressed. Research reported in this thesis was undertaken with the following objectives: Study of critical heat flux (CHF) and boiling heat transfer (BHT) enhancement mechanisms for dip-deposited graphene oxide coatings, effect of heater surfaces on boiling hysteresis and mechanism of partial reduction of graphene oxide.

## **1.4 Layout of the Thesis**

To meet the objectives outlined above, the following tasks were undertaken: Synthesis and characterization of graphene oxide as discussed in chapter 2, experimental setup and methods for pool boiling as discussed in chapter 3, and analysis of pool boiling experimental results as discussed in chapter 4. Summary of present research is given in chapter 5.

## Chapter 2

### 2 Synthesis and Characterization of Graphene Oxide

Graphene is an interesting material with exciting applications [19]. It has large theoretical surface area, high intrinsic mobility, high Young's modulus and thermal conductivity. It is a robust yet flexible membrane that allows infinite possibilities for modification or functionalization of the carbon backbone as discussed earlier in section 1.2.

Naturally occurring graphite is simply a stack of several layers of graphene that are bonded by Van der Waals force and are easily breakable compared to the lateral bonds that create the honeycomb structure of carbon atoms. Over the decades, the greatest challenge faced in graphene synthesis is obtaining a single or few layers of  $sp^2$  hybridized carbon atoms from naturally occurring graphite. Graphene derived from graphite can be chemically modified and has potential applications in composites and electrodes. These are named chemically modified graphene (CMG) or chemically converted graphene (CCG). Strong acids promote the oxidation of graphite, which in turn can be converted into chemically modified graphene (CMG) or graphene oxide (GO) upon exfoliation. This approach offers a great potential for manufacturing graphene oxide on a large scale [20].

Researchers have also produced thin samples of graphite by mechanical exfoliation techniques. Ruoff et al. [21] used Atomic Force Microscope (AFM) tip

to tear apart thin pillars from highly ordered pyrolytic graphite (HOPG) by plasma etching technique. The minimum thickness obtained was 200 nm which accounted for about 600 layers of graphene sheets. Kim et al. [22] used a micromechanical method to transfer the graphitic pillars onto a tipless cantilever, which was used to stamp down fewer sheets of graphene on a SiO<sub>2</sub> substrate. These were as low as 10 nm in thickness or approximately 30 layers of graphene. There were several other attempts to produce thin sheets of graphite over the years until 2004 when the scotch tape method was invented by Geim et al., who exfoliated monolayer graphene. This method just required a cellophane tape to remove graphene layers from graphite cake.

A review of the literature suggests that a major challenge faced in graphene synthesis is to develop an inexpensive, highly scalable and a simple method to exfoliate single or few layered graphene sheets from naturally occurring graphite. It is cumbersome to peel single layer large area graphene sheets from a graphite cake because of the weak Van der Waal force involved. During the mechanical tearing process, the graphene sheets normally isolate as multi-layer of sheets. Further isolating a mono-layer from such sheets is difficult. The mechanical, electrical and thermal performance of the material are mainly dependent on number of layers, method of synthesis and overall quality of the lattice structure. The available methods to produce nearly pristine graphene are briefly summarized in section 2.1.



## **2.1 Review of Graphene and nearly Pristine Graphene Synthesis**

The three major exfoliation techniques can be broadly classified as the classical scotch tape method, substrate-based synthesis and solution-based synthesis methods. While several methods to synthesize graphene are discussed in detail in literature; only select methods commonly used are discussed here.

### **2.1.1 Scotch Tape Method: Nobel Prize Winner**

Geim and his co-workers won the nobel prize for successfully exfoliating one-atom thick graphene sheet from naturally occurring graphite [23]. They used a commonly available cellophane tape to successively remove graphene layers from graphite cake, which was ultimately pressed down on the desired substrate to transfer the layers (this method is sometime referred to as the peeling method). Even though the number of layers were more than one, the weak Van der Waals force eventually resulted in a single layer graphene when the tape was lifted away. As one might expect, it is a slow and a difficult process, which requires experience for repeatable results. However, this technique resulted in a high quality crystalline structure. The limitation of this mechanical exfoliation technique is that it is difficult to obtain a large area single layer graphene on the substrate. This process is not scalable and cannot be directly applied in industries. However, it produced promising results that have served as a benchmark for other exfoliation techniques.

## **2.1.2 Substrate Based Synthesis**

The two main types of substrate-based synthesis methods are epitaxial graphene and chemical vapor deposition.

### **2.1.2.1 Epitaxial Graphene**

De Heer et al. [24] pioneered a method of growing multi-layered graphene epitaxially, which resulted from high temperature reduction of monocrystalline silicon carbide. Silicon was desorbed at a temperature of 1000° C in high vacuum conditions leaving behind islands of few layers of honeycomb carbon structures on the silicon carbide surface. Scanning Tunneling Microscopy (STM) and electron diffraction experiments were conducted to characterize the graphene monolayer structure. It was also found that epitaxial graphene could be patterned using standard lithography techniques, which in turn were used to make nano-electronic devices. Since, the graphene was grown on a substrate, it was named as substrate-based synthesis method.

### **2.1.2.2 Chemical Vapor Deposition**

The second available substrate-based methodology is the chemical vapor deposition (CVD) process. Reina et al. [25] exposed polycrystalline Ni films to a highly diluted hydrocarbon flow at 900 to 1000° C under ambient pressure conditions to produce single- to few-layer graphene. The Ni films were e-beam evaporated onto Si or SiO<sub>2</sub> substrate. The graphene growth in this process was

attributed to the precipitation of graphite from carbon species within the transition metal like Ni. As the solubility of carbon in Ni was temperature-dependent, the graphene layer precipitated upon cooling of the sample. The major advantage of the substrate-based graphene synthesis techniques is its scalability and high compatibility in integration with the present CMOS technology.

Briefly, both the epitaxial and CVD growth of graphene have the potential of forming single crystal of graphene on semiconductor chips. However, the major difficulty faced during both of these substrate-based growth methods was the ability to produce uniform crystal growth throughout the exposed substrate area without allowing the formation of grain boundaries.

### **2.1.3 Solution Based Synthesis**

The solution based synthesis of graphene was first shown by Ruoff et al. [26]. In this approach, a water dispersible intermediate compound called graphite oxide was synthesized by Hummer's method—a wet chemical synthesis method and an effective oxidation process [27]. The underlying principle in this method is that the layered stack of graphite oxide can be exfoliated by the application of mechanical energy such as in a sonication bath. The hydrophilic nature of graphene oxide sheets lets water to readily intercalate between the sheets and disperse as individual graphene oxide platelets. Graphene oxide can also be further processed to form self-assembled graphene oxide paper of desired area as discussed in section 2.3.

The as-synthesized graphene oxide is also called as chemically modified graphene (CMG) or chemically converted graphene (CCG). The detailed description of the chemical synthesis adopted in this research is explained in the following sections.

Solution-based synthesis of graphene oxide has proven to be highly scalable and an easily controllable chemical process. Based on the review presented above, solution-based approach was selected as the appropriate method for graphene oxide synthesis.

## **2.2 Laboratory Synthesis of Graphene Oxide**

The steps involved in the synthesis of chemically converted graphene are as follows:

- **Step 1:** Chemical oxidation of naturally occurring graphite by Hummer's method
- **Step 2:** Filtering and washing of as-oxidized graphite
- **Step 3:** Mechanical exfoliation of oxidized graphite by ultra-sonication
- **Step 4:** Dip and spray-coating of exfoliated and dispersed graphene oxide

### **2.2.1 Hummer's Method**

It is a highly scalable and an economical process, and the material that results from this process is called graphite oxide whose layers can be easily

exfoliated by sonication. All the raw materials required for this process were purchased from Sigma Aldrich®.

The synthesis of graphite oxide paste was carried out in three temperature stages. Three hundred milligrams of naturally occurring graphite powder and 150 mg of sodium nitrate salt ( $\text{NaNO}_3$ ) were added to 10 mL 98% concentrated sulphuric acid ( $\text{H}_2\text{SO}_4$ ) in a 100 mL Erlenmeyer flask. The mixture was then stirred in a magnetic stirrer for 4 hours. The flask was then placed inside an ice bath maintained at temperature  $< 5^\circ \text{C}$ . Nine hundred milligrams of potassium permanganate ( $\text{KMnO}_4$ ) were added to the mixture gradually over 30 minutes. An exothermic reaction took place upon addition of  $\text{KMnO}_4$  and produced highly inflammable fume. To avoid any explosion, the beaker containing the reactive mixtures was maintained at very low temperature (below  $5^\circ\text{C}$ ) and  $\text{KMnO}_4$  was added gradually to avoid rapid production of flammable fume. After completely adding  $\text{KMnO}_4$ , the mixture was stirred for additional 4 hours, and it turned deep green at that point. This marked the end of low temperature stage. The flask was then transferred to a water bath maintained at 40 to  $45^\circ \text{C}$ , and the mixture was stirred continuously for 2 hours at that temperature. Twenty eight milliliters of distilled water was added drop by drop to the as-formed slurry while continuously stirring the mixture. As the water droplets mixed with the slurry, it formed brown colored streaks that indicated the formation of graphite oxide, which can be easily loosened to form graphene oxide. Upon addition of 28 mL of distilled water, the

mixture was further stirred for 2 hours at that stage. It formed a dark brown solution, which marked the end of medium temperature stage. Finally, the flask was transferred to a water bath maintained at 90° C and stirred for additional 2 hours at the high temperature stage. At the end of this stage, oxidation process was terminated by adding 18 mL of 30% hydrogen peroxide (H<sub>2</sub>O<sub>2</sub>). The resulting product was then filtered and washed as discussed in the next section.

### **2.2.2 Filtering and Washing of Oxidized Graphite**

The resulting solution was stored for 24 hours to form a sedimentation of graphite oxide paste at the bottom leaving behind a clear solvent at the top. The clear solvent contained most of the sulphuric acid and salt impurities, which were then removed by sucking them from the top using a pipette or syringe. The resulting graphite oxide paste was again diluted with water, and the same process was continued for four to five times. The as-produced paste was then washed and filtered with 5% hydrochloric acid (HCl) twice to remove any salt impurities. The resulting graphite oxide paste can be dispersed readily in water for coating applications.

### **2.2.3 Mechanical Exfoliation by Ultra-Sonication**

A concentration of 0.5 mgmL<sup>-1</sup> was used. For instance, 30 mg of graphite oxide was mixed with 60 mL of distilled water, and the mixture was sonicated in a BRANSON® sonication bath for 60 min. The sonication process mechanically

exfoliated the already-loosened graphite oxide layers and resulted in uniform dispersion of graphene oxide platelets in water. The as-synthesized dispersion could be coated onto the substrate of interest for research purposes.

To study the stability of graphene oxide nanosheets dispersion in water, the prepared colloids were stored in vials for sedimentation test to check for any sedimentation. It was observed that there was no evidence of any sedimentation even after four weeks of dwell time. Because of the super hydrophilic nature of the graphene oxide nanosheets, a good colloidal suspension was formed, which could be used for further processing.

#### **2.2.4 Coating of Graphene Oxide**

Graphene oxide platelets were transferred to the substrates of interest using dip coating and spray coating techniques.

##### **2.2.4.1 Dip Coating Process**

Dip coating is one of the oldest thin film deposition processes available among the wet chemical deposition methods. The as-synthesized colloidal solution of known concentration ( $0.5 \text{ mgmL}^{-1}$ ) was used for the dip coating process.

Dip coating was carried out on NiCr wire samples for conducting experiments in the pool boiling setup described in the following chapter. The main parameters involved in dip coating process are graphene oxide colloid concentration, type of organic solvent, immersion time and number of cycles of

coating. After several trials for producing uniform coating of graphene oxide, the number of coating cycles and the concentration of organic solvent were fixed at 50 and  $0.5 \text{ mgmL}^{-1}$  respectively. Deionized water was used as the organic solvent. Since graphene oxide is hydrophilic, it formed a uniform dispersion. The immersion time for the dip coating process was fixed at 5 seconds. The process can be separated into three main technical stages.

**Immersion and dwelling:** The NiCr wire, which was connected to electrodes was immersed into the GO suspension followed by a dwell time of 5 seconds for ensuring sufficient interaction between the wire surface and graphene oxide platelets, and provide complete wetting. Graphene oxide contained carboxylic end groups, which greatly reduced the surface tension of the solvent and significantly lowered the wetting time for coating process.

**Deposition and drainage:** The NiCr wire was taken out of the colloidal suspension. At this stage, a thin layer of liquid suspended with graphene oxide platelets was trapped on the surface of the wire and the excess solution was drained into the bath. This process resulted in deposition of a thin layer of graphene oxide platelets.



**Evaporation:** The as-deposited thin layer of coating contained residual water that had to be evaporated. The wire was Joule heated by DC current supply for 20 seconds to remove water molecules from the surface, leaving behind a dry thin layer of graphene oxide deposition. The above steps were carried out for 50 cycles

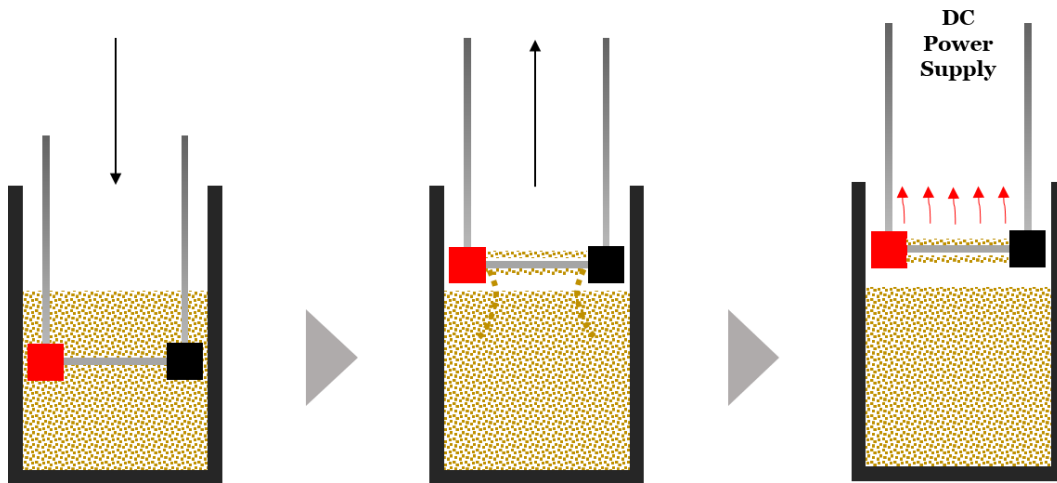


*Figure 2:1 Dip coating of graphene oxide on NiCr wire: A representative picture*

of coating to obtain sufficient coating thickness. The schematic of the dip coating process is shown in the Figure 2:1.

#### **2.2.4.2 Spray Coating Process**

Spray coating process is also a wet thin film deposition process that has been employed in the current research. An air brush sprayer with nitrogen gas was used for spray coating graphene oxide onto flat surfaces. The flat substrates used were silicon dioxide wafer, copper coupons and aluminum foil. The spray-coated materials were characterized using Scanning Electron Microscopy (SEM) imaging

and Raman spectroscopy techniques as discussed in section 2.3. The parameters associated with spray coating process are concentration of colloidal suspension, spraying time, dwelling time, post baking temperature and spraying distance. After a number of trials for producing a fairly uniform deposition, the concentration, spraying time and dwell time were fixed at  $0.5 \text{ mgmL}^{-1}$ , 3 seconds and 20 seconds respectively. The post baking temperature was set at  $200^{\circ} \text{C}$  to enable evaporation of embedded water molecules. The spraying distance, which is defined as the distance between tip of nozzle and the substrate, was fixed at 25 cm. The two main technical stages involved in spray coating process are spraying and post-baking.

**Spraying:** The colloidal suspension was sprayed onto the substrate of interest placed on a hot plate at  $200^{\circ} \text{C}$  for 3 seconds. The schematic of the spraying process used is shown in Figure 2:2. The substrate was dwelled for 20 seconds before the

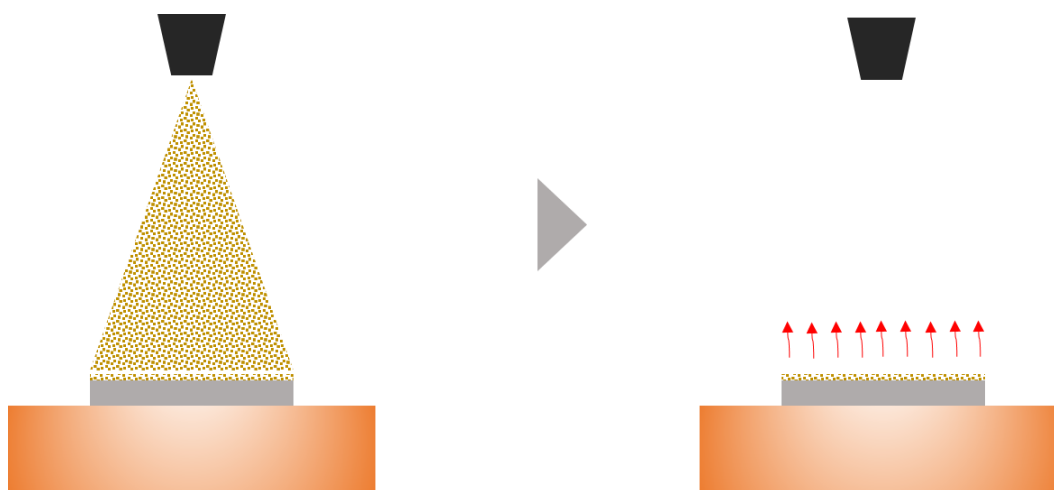


*Figure 2:2 Spray coating of graphene oxide on flat substrates: A representative picture*

next spray. The spraying process was carried out for 50 cycles before it was taken for post-baking.

**Post-baking:** The substrate was dried at 200° C for 30 minutes on a hot plate to ensure complete evaporation of water molecules trapped inside the self-assembled porous layer of graphene oxide.

It is noted that the NiCr wires used for studying boiling process were coated only by dip coating process. Spray coating was not employed as it resulted in non-uniform coating along the surface.

### **2.3 Characterization of Graphene Oxide**

Graphene oxide papers were produced from the concentrated graphite oxide dispersions obtained from the chemical synthesis process. The concentrated dispersion of graphite oxide was transferred onto a glass petri dish and dried in vacuum oven at 60° C for 24 h. After completion of the drying process, the graphene oxide paper could be simply peeled off from the glass surface. The GO papers produced by the above method were dark brown in color, which is the characteristic color of graphene oxide. These were mainly synthesized for characterization purposes and could be completely or partially reduced in an inert atmosphere at a range of temperatures. The representative picture for the process is shown in the Figure 2:3.

The processed graphene oxide coatings and graphene oxide papers were characterized using Raman spectroscopy, Scanning Electron Microscopy (SEM), and Atomic Force Microscopy (AFM) techniques.

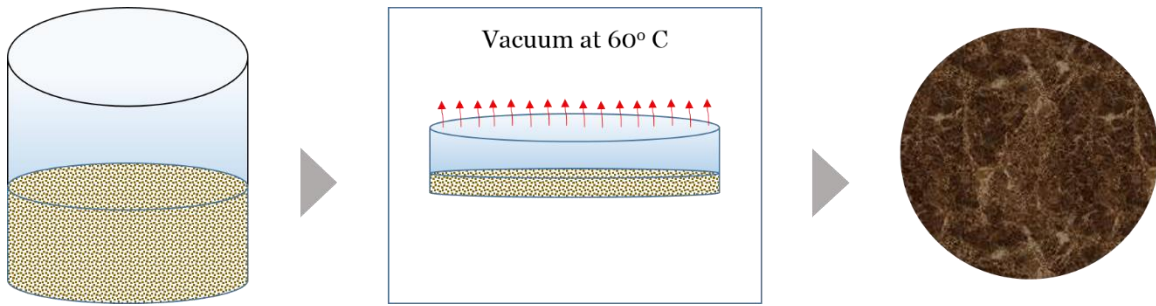


*Figure 2:3 Preparation of graphene oxide paper: A representative picture*

### **2.3.1 Raman Spectroscopy**

Raman spectroscopy is widely used for characterizing graphene and graphene based materials as they contain  $sp^2$  hybridized carbon atoms [28]. The  $sp^2$  hybridized carbon atoms can be represented in great details using this characterization technique.

The distinct bands involved in the Raman spectra of graphene and graphene-based materials are the G-band, D-band and the 2D- band.

**G-band:** G-band is the primary mode of in-plane vibration in graphene and graphite. It is caused by the vibration of  $sp^2$  hybridized carbon atoms arranged in a planar configuration as shown in Figure 2:4. Unlike other bands, the G-band is independent of the excitation laser frequency. The band width and position of the band provide information on the layer thickness for a pristine graphene. However,

any impurities present in the pure graphene affect the results. Thus, Raman spectroscopy cannot be used to characterize layer thickness for chemically synthesized graphene oxide as it may contain salt residuals, carboxylic and functional oxygen groups.

**D-band:** The D-band, otherwise called as the disorder band or defect band, is the result of the carbon ring breathing mode and elastic scattering that are initiated in the vicinity of any defect, edge or disorder in the graphene sheet. The D-band is either weak or completely absent in graphite and pristine graphene. However, graphene oxide and reduced graphene oxide may contain number of defects that vary based on the method of synthesis and reduction techniques used. The defect band is therefore significant in the aforementioned materials, and can be used to study the mechanism of reduction process through careful observation of changes in D-band at various stages of reduction. The intensity of D-band is proportional

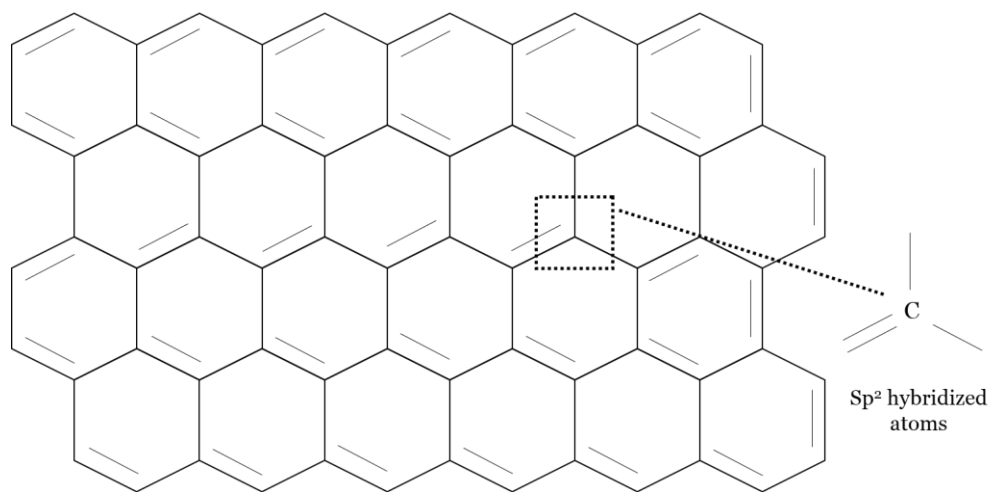


*Figure 2:4 SP<sup>2</sup> hybridized carbon atoms in a sheet of graphene: A schematic representation*

to the amount of defects in the material. Unlike G-band, the important thing to be noted about the D-band is that it is sensitive to the type of excitation laser used. Hence, it is required to use the Raman spectroscopy under same input conditions for characterizations done using D-band. Since G-band is independent of excitation frequencies, the defects can be characterized by using the intensity ratios of G and D-bands:  $I_D/I_G$ .

**2D-band:** The 2D-band is the second order of the D-band and is commonly referred as the overtone of D-band. It is the result of two phonon lattice vibrations and is not initiated by a defect or disorder in the sample. Even a pristine graphene shows a 2D-band in the Raman spectrum. The significance of 2D-band is that it can also be used to determine the layer thickness but only for pristine graphene and not for other graphene-based materials derived from naturally occurring graphite. From literature, it can be noted that the layer thickness can be determined by taking the ratio of intensities of 2D-peak and G-peak ( $I_{2D}/I_G$ ). Since chemically-synthesized graphene oxide samples were used for characterizations, 2D band and its significance on graphene oxide samples were not studied in the characterization technique discussed in this section.

The as-prepared graphene oxide paper was cut into samples of 5mm x 5mm size, which were used for carrying out Raman characterization. Raman spectroscopy experiments were conducted at room temperature using a 785 nm excitation laser in a WITech® Raman microscope. This Raman instrument consists of an excitation Ar laser of 785 nm wavelength, light collection optical microscope of up to 100x magnification capability, and a “super-notch-plus” filter for eliminating elastic light. The scattered photons from the graphene oxide sample were analyzed using a monochromator that was connected to a liquid nitrogen cooled CCD. The Raman spectra was finally plotted in an intensity vs wavenumber or Raman Shift ( $\text{cm}^{-1}$ ) graph. The characteristic Raman spectrum for the as-synthesized graphene oxide is shown in the Figure 2:5.

Two bands namely G-band and the D-band were investigated by Raman spectroscopy. The G-peak position of the graphene oxide sample occurred at a

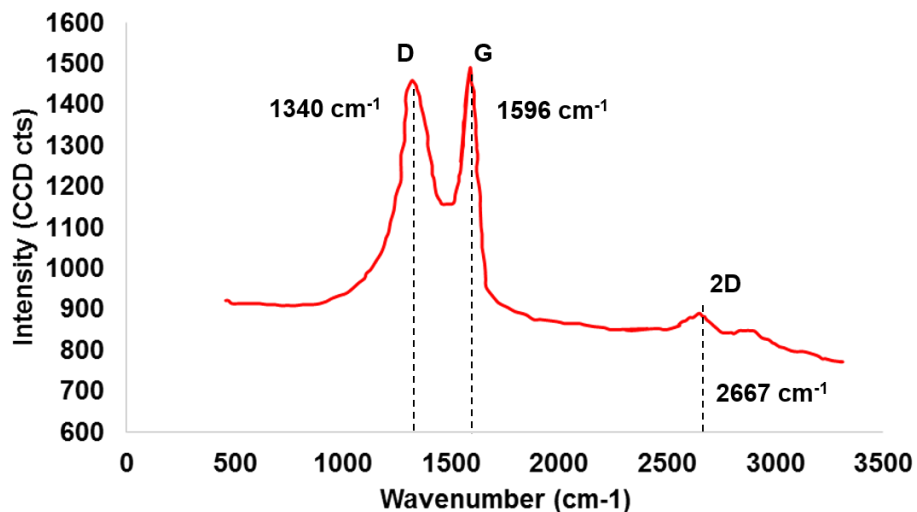


Figure 2:5 Raman spectrum of graphene oxide paper

wavenumber of  $1596\text{ cm}^{-1}$  and the D-peak at  $1340\text{ cm}^{-1}$ . The intensity ratio of D-band to G-band ( $I_D/I_G$ ) that gives an information on the amount of defects present in the sample was found to be 0.97. This ratio is expected to go up as the reduction takes place. This is due to the reduction in the sizes of  $\text{sp}^2$  sheets in the material during the reduction process. The positions of D-band and G-band are highly sensitive to the synthesis method and excitation laser used. However, the overall behavior of the graphene oxide samples is in good agreement with the Raman spectrum for graphene oxides found in literature.

### **2.3.2 Scanning Electron Microscopy**

Field Emission Scanning Electron Microscope (FESEM) was used for imaging the graphene oxide-coated surfaces. The heated wire dip-coated with graphene oxide, aluminum foil spray coated with graphene oxide and graphene oxide paper were used for studying surface topography. The SEM images of the GO surfaces coated on NiCr wire and Al foil samples, in that order, at various magnifications are shown in Figure 2:6 and Figure 2:7. It is seen from the images that graphene oxide forms a self-assembled porous and nano-rough surface, which



can significantly improve fluid permeability and capillary wicking action. The SEM images also reveal bending and folding of as-deposited graphene oxide sheets that give rise to nano-scale roughness to the surface. The surface topology and its effects

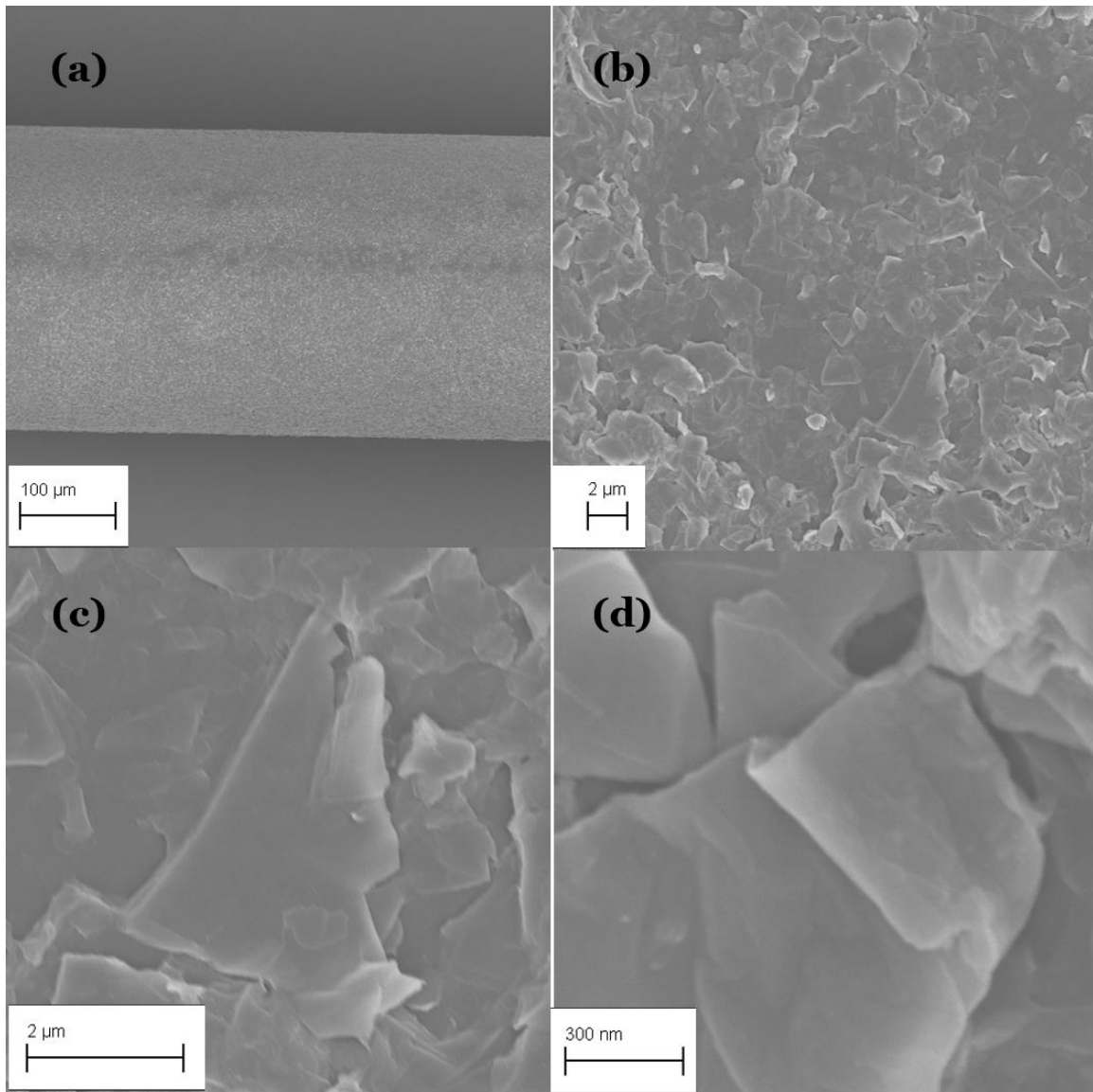


*Figure 2:6 SEM Images of graphene oxide layers on NiCr wire at various magnification levels (a) represents uniform coating of dip-deposited GO on NiCr Wire, (b) and (c) shows the self-assembled porous structure and (d) shows the bending of graphene oxide sheet that induces nano-roughness.*

on boiling heat transfer and critical heat flux enhancements are discussed in further detail in chapter 4.

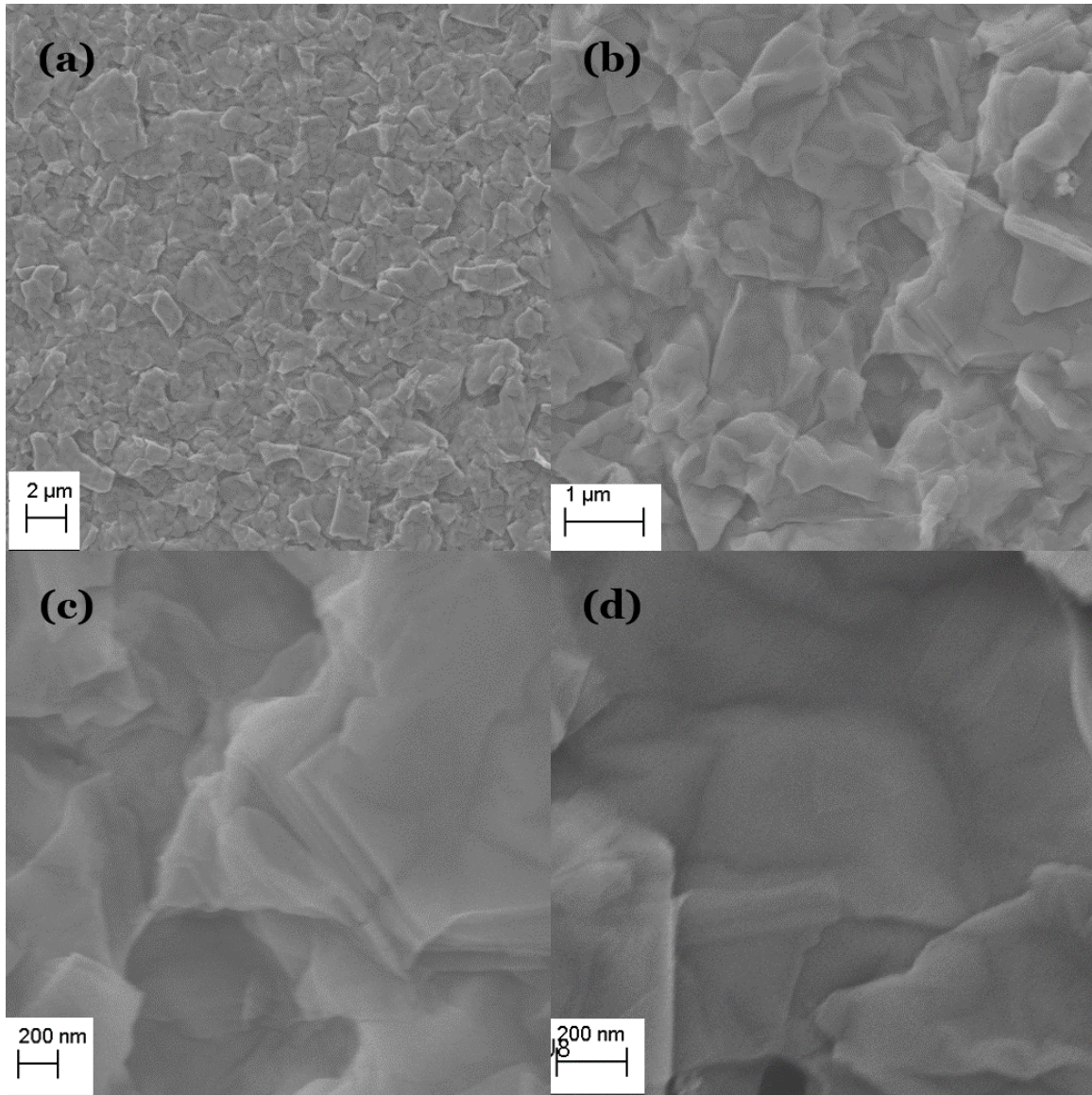


*Figure 2:7 SEM Images of graphene oxide paper at various magnification levels. (a) and (b) clearly shows the characteristically ordered porous surface. (c) Shows the layers of graphene oxide stacked on one another.*

### 2.3.3 Atomic Force Microscopy

Atomic force microscopy is a high resolution scanning probe microscopy with resolution on the orders of fractions of nanometers. The heating surface dip-coated with graphene oxide was analyzed by AFM technique to quantify surface roughness and average thickness of coating. Figure 2:8 shows the surface topology of graphene oxide coating across an area of  $25\ \mu\text{m}^2$ . The measured arithmetic mean of surface deviation ( $R_a$ ) was 460 nm for dip-coated graphene oxide. There was a certain length of wire (about 4 mm) which was not coated during the dip coating process as it was covered by the end clips connecting the wire to the power supply. To measure the thickness of the wire, the scanning probe was traversed from the uncoated surface through the coated surface, and the deviation from surface was

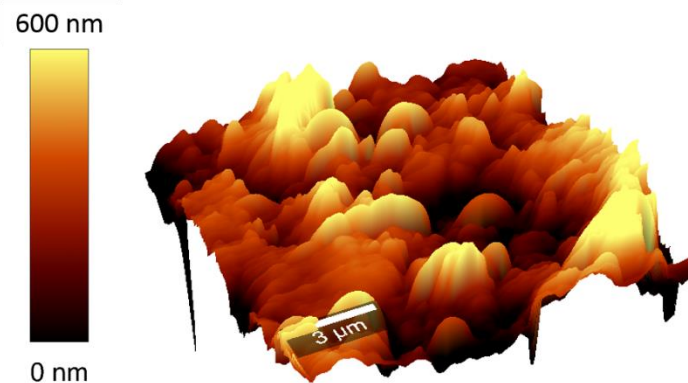


*Figure 2:8 Surface topology of graphene oxide coatings on NiCr wire. The heat map clearly depicts the nano and micro-roughness of porous graphene oxide layer assembled on the surface*

measured. The measured average thickness of graphene oxide coating was 860 nm. The thickness of coating is essential to quantify thermal activity, the ability of material to spread heat, which can be used to understand the enhancement mechanisms of critical heat flux. All AFM characterizations were performed using a WITech® Atomic-force Microscopy. As shown in Figure 2:8, graphene oxide coating forms a self-assembled rough and porous layer, which could have prominent effect on convective heat transfer coefficient in nucleate boiling regime.

## Chapter 3

### 3 Pool Boiling Experimental Setup and Methods

The objective of this chapter is to describe the heater sample preparation methods, temperature-resistance calibration of nichrome wires, and pool boiling experimental setup and methodologies.

#### 3.1 Heater Sample Preparation

NiCr wire was the base heating material used for all the experiments as they are available at low cost and have high melting temperature. The three main types of specimens used for pool boiling experiments were bare wires, sand paper-scratched wires and graphene oxide-deposited wires. The Table 3-1 summarizes the types of heater surfaces used, and their preparation methods.

All the wires were 0.501 mm in diameter and 50 mm in length. Around 60 samples of bare wires of aforementioned dimensions were prepared for experimental purposes. The wires were annealed at 200° C for 4 hours to relieve

*Table 3-1 Heater wire samples for pool boiling experiments*

<b>Sample</b>	<b>Preparation Method</b>	<b>Convention</b>
Bare NiCr Wire	Directly after annealing	BW
Scratched Wire	80 Grit Sand Paper	SW
Graphene Oxide Coated Wire	50 Cycles of Dip Coating	GO 50

any thermal stress that might have been induced during wire straightening process. It also improved the repeatability of the results obtained during the pool boiling experiments.

Five samples from the bare wires were scratched with 80 grit aluminum oxide sand paper for creating surface roughness. Thirty wires were coated with graphene oxide using dip coating process discussed in section 2.2.4.1. The dip deposition was carried out for 50 cycles of coating. For surface characteristics of these wires see section 2.3.

### **3.2 Resistance –Temperature Characterization for Heating wire**

All the pool boiling experiments were conducted using 24 gage or 0.501 mm nickel chromium wire heaters with a composition of 80% nickel and 20% chromium, and were purchased from McMaster-Carr®. Resistance – temperature calibration for the NiCr wires was carried out to determine the temperature-resistance co-efficient, which in turn can be used to calculate the temperature of the wire by measuring the resistance across it.

#### **3.2.1 Experimental Configuration and Method for Temperature-Resistance Calibration**

The experimental setup to conduct temperature-resistance characterization of NiCr wire is shown in the Figure 3:1. It consists of a 1000 mL Pyrex beaker filled with deionized water at constant temperature, a Thermo Scientific® hot plate

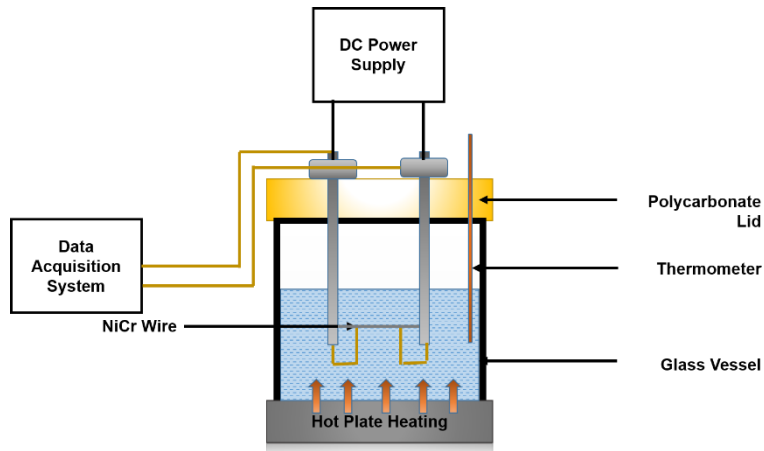


*Figure 3:1 Experimental setup for resistance-temperature characterization of NiCr wire*

heater, Agilent® 6V 5A DC power supply and a Keithley® nano-voltmeter accurate up to  $\pm 1\text{nV}$ . All experiments were conducted at atmospheric conditions.

A NiCr wire of length 50 mm and diameter 0.501 mm was connected to a DC power supply and immersed in the constant temperature water bath. The Pyrex glass was filled with 500 mL of deionized water and heated to a constant temperature, which was continuously monitored by a K-Type immersion thermocouple placed in the water bath. The resistance of the wire was measured at different temperatures from 20° C to 90° C in steps of 10° C. When a steady state was reached for a particular value of temperature, the voltage across the wire was measured for 5 different values of input current in mA range, so that joule heating effect was eliminated. From these 5 reading, the mean value of the resistance was found. The resistance of the wire was found by using the simple Ohmic relation:

$$R_w = \frac{V_w}{I_c}$$

where  $R_w$  is the resistance of the wire,  $V_w$  is the voltage across the wire and  $I_c$  is the circuit current.

The resistivity was calculated as follows:

$$\rho_w = \frac{R_w A_w}{L_w}$$

where  $A_w$  and  $L_w$  are the cross sectional area and length of the wire respectively. The normalized resistance ( $R_{w,T}/R_{w,20}$ ) was plotted against the temperature difference ( $T-T_{20}$ ) as shown in Figure 3:2. A linear fit estimated the value of temperature-resistance coefficient to be  $0.00015 \text{ K}^{-1}$ , which lies within the known

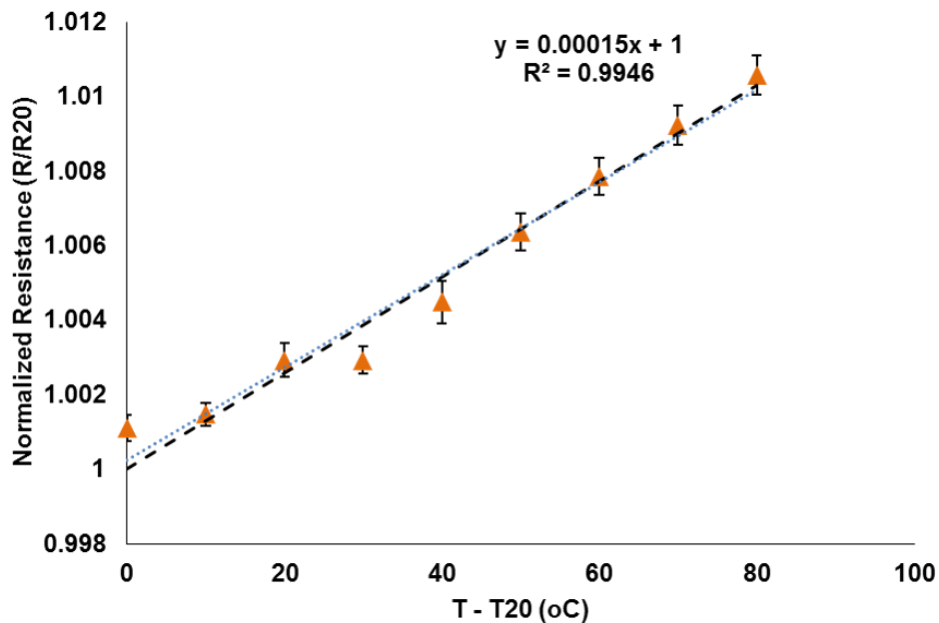


Figure 3:2 Resistance-temperature characterization plot for NiCr wire



range of values for thermal expansion coefficients for NiCr wires from properties table.

The value of temperature-resistance coefficient, so determined, was used to determine temperature of the wire by comparing the equation of linear fit to the resistance-temperature relation shown below:

$$\frac{R}{R_{20}} = \alpha(T - T_{20}) + 1$$

### 3.3 Pool Boiling Experimental

The schematic diagram of the pool boiling setup is shown in the Figure 3:3. The experiments were conducted in a Pyrex glass vessel at atmospheric pressure conditions. Due to very low thermal conductivity of the Pyrex glass material, it blocked the heat loss to the surroundings, and maintained the working fluid at the

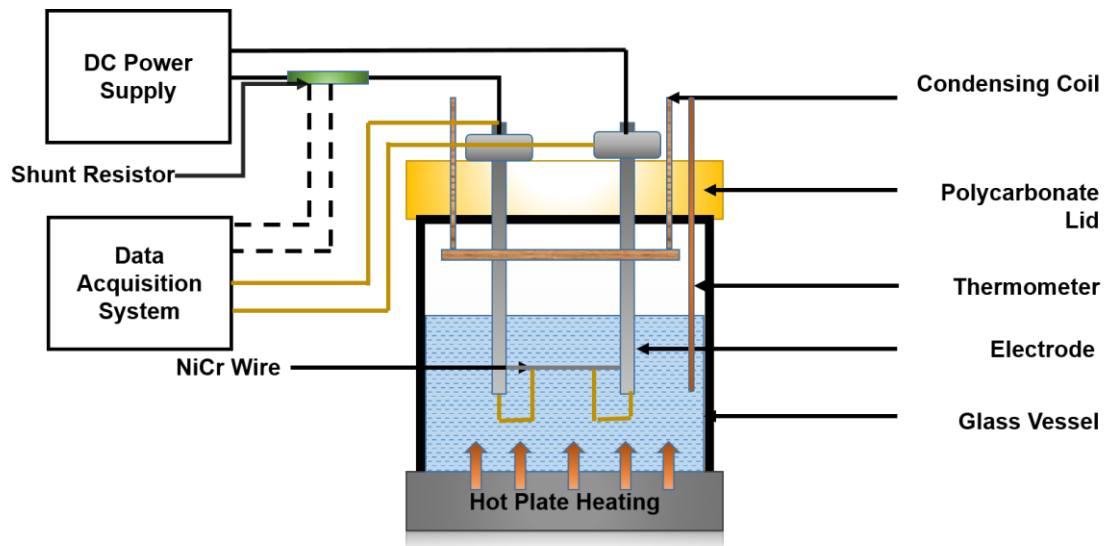


Figure 3:3 Pool boiling setup

desired temperature, which is saturation temperature in this case. Since the Pyrex vessel is transparent, it aided in visualization of the pool boiling process using high speed (fps) cameras. A Discovery Veho® USB microscope was used to visualize the bubble dynamics as the pool boiling experiment progressed. As mentioned before, NiCr wire was used as the base heater material in all pool boiling experiments.

The NiCr wire was heated using a 15 V 60 A Tenma® DC power supply using Joule heating method. Stainless steel rods were used to avoid corrosion, and entry of foreign impurities, such as rust, into the working fluid. The connectors that held the NiCr wire were 3-D printed to required dimensions and were made of plastic material with high temperature resistance. NiCr wires of length 50 mm and diameter of 0.501 mm were used in all experiments. Copper wires were soldered to the NiCr wires at a distance of 15 mm from the ends to measure the voltage across the heater of known length.

The Pyrex glass beaker was filled with FC – 770, a heat transfer fluid purchased from 3 M. The saturation temperature observed at room temperature was 95° C ( $T_{sat}$ ). At room temperature, a fixed distance of 20 mm was maintained between the surface of the working fluid and the heater wire. A copper condensing coil was fixed to the polycarbonate lid for recirculating the evaporated fluid back to the pool. A Thermo Scientific® hot plate heater was used to raise the temperature of the working fluid to its saturation temperature. A K-type immersion

thermocouple was used to continuously monitor the fluid temperature to make sure it was fixed at the saturation temperature.

To start the pool boiling experiment, the temperature of hot plate was raised to saturation temperature of FC 770. Using the Tenma DC power supply, current was supplied in steps of 0.1 A until the critical heat flux point was reached. The heater temperature was determined from the resistance measured across the wire, as discussed above. Uncertainty analysis in the pool boiling experiment was carried out using error propagation method of Kline and McKlintock [29].

A NI® 441 cable was connected to the nano-voltmeter to acquire data automatically at each current step. A MATLAB code was used to operate the data acquisition cable. The critical heat flux point was marked by a sudden drop in the supply current, or an overshoot in the voltage across the wire. It is not safe to operate beyond this point as it may cause heater failure by sagging and melting.

Boiling curve for a bare NiCr wire in a pool of saturated FC 770 is shown in the Figure 3:4. It is noted that the CHF of FC 770 is in good agreement with the CHF values of other Fluorinert fluids, which are similar to FC 72 and FC 77 reported in literature.

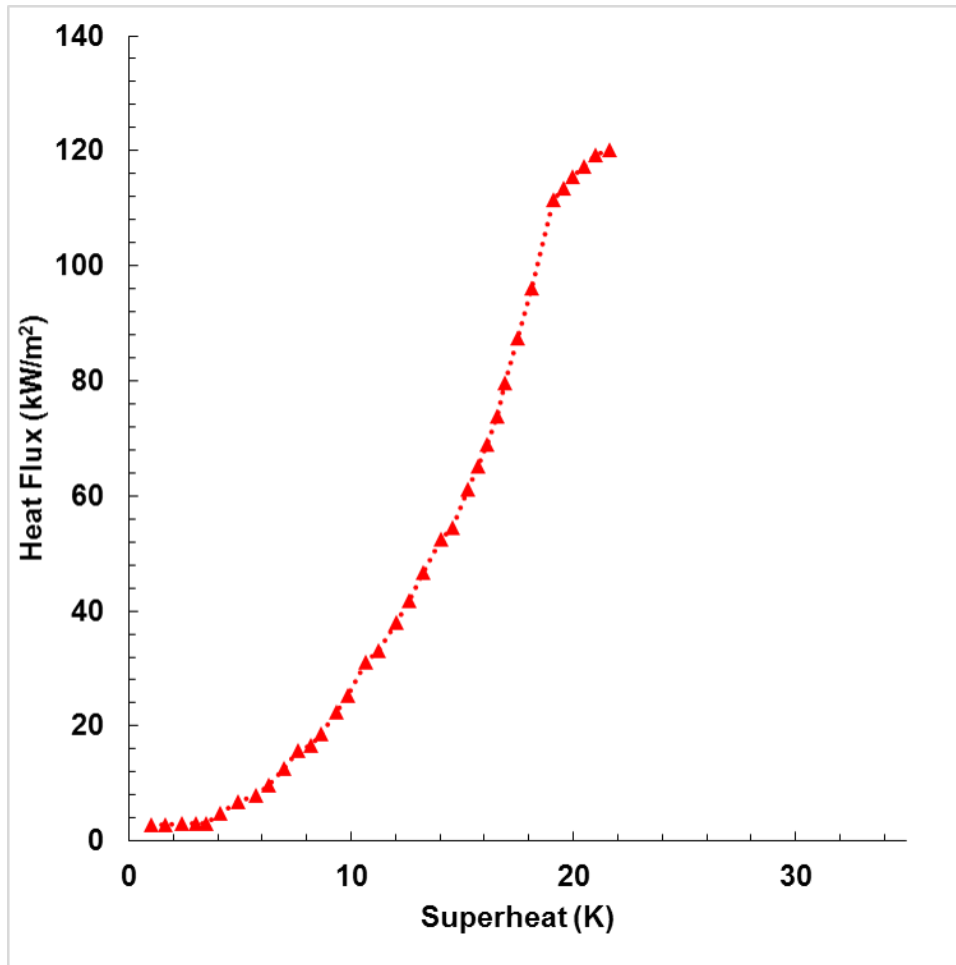


Figure 3:4 Boiling curve for bare NiCr wire in FC-770 until the critical heat flux was reached

## Chapter 4

### 4 Experimental Results and Discussions

This chapter will focus on the pool boiling experimental results and analysis for bare, scratched and graphene oxide-coated wires. The first section deals with boiling curve hysteresis analysis where the effects of surface morphology on incipient pool boiling are studied. The second section explains the complete boiling curve for all the three heating surfaces. A parametric sensitivity analysis to explain the mechanisms of CHF and BHT enhancement mechanisms is reported in section 3. In section 4, primary attention is given to observing the partial reduction mechanism of graphene oxide and its effects on CHF enhancement.

#### 4.1 Hysteresis Analysis

A common observation in pool boiling of highly wetting fluids on smooth surface is the presence of hysteresis, which is accompanied by a temperature overshoot at the onset of nucleate boiling point. Vapor embryos trapped in the cavities that are distributed on the heater surface act as the nucleation sites to commence boiling [30]. The Gibbs-Thompson equation relates the pressure and interface curvature in a system at equilibrium as follows:

$$p_l - p_g = \frac{2\sigma}{r}$$

where  $r$  is the radius of embryo bubble,  $p_l$  is the liquid pressure,  $p_g$  is the vapor pressure and  $\sigma$  is the interfacial surface tension. From the above relation, it is noted that a higher wall superheat is required to promote bubble growth and release of smaller vapor embryos. When the heater is immersed in a pool of stagnant fluid, it floods the heater surface suppressing the number of active boiling centers or embryos and gives rise to temperature overshoot. Wettability greatly influences the fluid penetration characteristics and affects the extent of temperature overshoot. A well-wetting fluid is expected to cause a higher overshoot temperature than a low wetting fluid. Another parameter that is expected to have control on this behavior is the surface roughness. Increased roughness decreases the superheat for the pool boiling to instigate and restricts temperature overshoot [31].

Delay time is defined as the time taken for the working fluid to completely flood the heater surface and/or penetrate through the porous structures in the heater [32]. For a highly wettable fluid like FC 770, it is expected that the delay time is very small thereby increasing the risk of hysteresis. Incipient boiling point is the heat flux above which the bubble nucleation takes place efficiently. The implications of hysteresis effect in practical applications are: for any constant heat flux system, it is safer to operate the system at a heat flux greater than that at the nucleate boiling incipient point. Likewise in a constant temperature system, the

superheat corresponding to the incipient point should be exceeded. An ideal heater surface is one which eliminates the phenomenon of hysteresis.

In 1982, Bergles et al. [32] reported hysteresis effects in the heating curves for water and R-113 on porous metallic coatings. They noted hysteresis in both moderately wetting fluids like water and highly wetting fluids such as R-113. It was observed that the previous history and temperature of heating surface and the continuous or stepwise increment in the heat flux affected the extent of temperature overshoot and resultant boiling curve hysteresis. They proposed that the simplest way of avoiding hysteresis problem was to supply a high heat flux, or start the boiling process at a higher superheat.

Marto et al. [33] conducted boiling experiments on three enhanced copper surfaces using FC 72 and R-113. Anderson et al. [31] studied the pool boiling characteristics of a simulated microelectronic chip in a stagnant pool of FC 72 fluid. In both these studies, they reported a similar dependence of incipient point on the previous history and temperature of heating surface. Athreya et al. [34] studied the pool boiling of FC 72 on metallic foams and reported the effects of orientation and geometry on temperature overshoot and hysteresis. They observed that the effect of hysteresis increased with reduction in the height of metallic foam in the horizontal orientation.

From the above review of literature, it is clear that the risk of temperature overshoot is prevalent with highly wettable fluids like FC 72 and FC 770. The study of hysteresis effect is thus an essential aspect in pool boiling heat transfer analysis.

To observe the effect of heating surfaces on hysteresis and temperature overshoot, new samples of bare wire (BW), scratched wire (SW) and graphene oxide coated (GO50) wires were used. The maximum heat flux supplied to the wire was kept at around 50% of critical heat flux (CHF) of the corresponding heating surface, where the CHF values were determined by conducting pool boiling experiment as discussed in section 3.3. The rationale for selecting ~50% CHF value is as follows. If the wire were to be heated to the CHF point, it would have experienced a sudden increase in temperature on the order of a few hundred degrees Celsius. The accompanying annealing on the wire has the effect of trapping vapors on the surface which act as nucleating spots thereby eliminating hysteresis effect. Since, the surface temperature history and heat treatments have effect on hysteresis as discussed above, previously used heating wires are not appropriate to study the hysteresis effect. In order to operate the heater at an input heat flux of around 50% CHF, the CHF values of different heater surfaces were determined by conducting pool boiling experiments.

#### **4.1.1 Critical Heat Flux for Various Heating Surfaces**

As mentioned in Table 3-1, the heating surfaces BW, SW and GO50 were used. During the pool boiling experiments, the critical heat flux was always



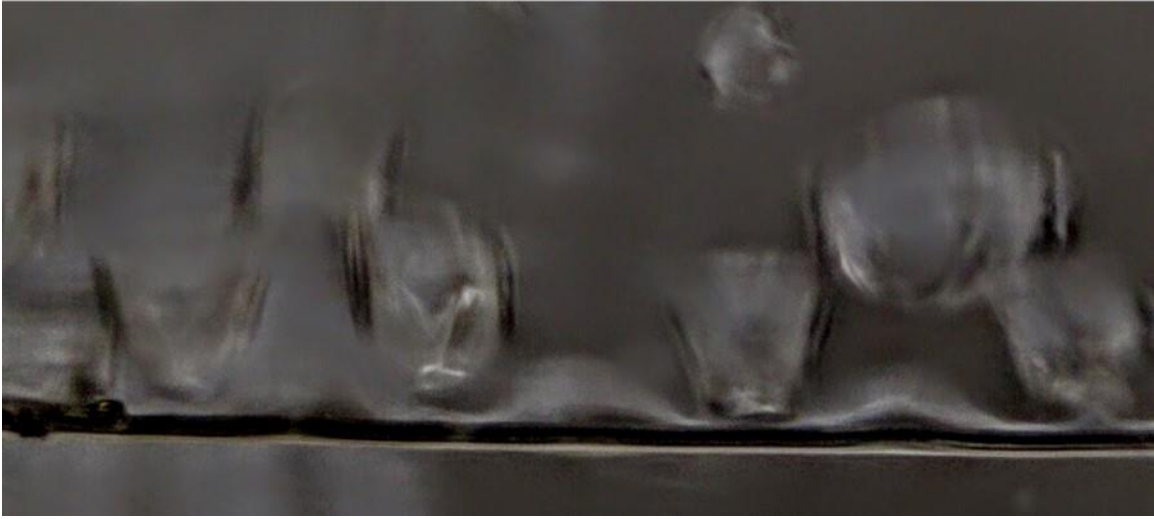


*Figure 4:1 Visualization of bubbles coalescing just after the CHF point is reached on a bare NiCr wire*

accompanied by a rapid increase in the heater wall temperature, which was indicated by a rise in wire resistance measured by nano-voltmeter. When the critical heat flux point was reached, the bubbles formed on the heater surface coalesced and formed vapor film around it, as shown in Figure 4:1. At this stage, called as the transition boiling regime, the proportion of film boiling region along the heater surface rapidly increased. As a result, the temperature of the heater surface ramped to a higher value due to the loss in effective heat transfer from the heater to the surrounding vapor, which had significantly low thermal conductivity and associated heat transfer coefficient. The heat flux at film boiling regime could be captured without burnout of the wire, when the input current was carefully monitored. All the pool boiling experiments were conducted with horizontal orientation of the heater wire. The experimental values of critical heat flux observed for FC 770 on BW, SW and GO50 are reported in the Table 4-1. The

average CHF value for bare wire (BW) was 118.5 kW/m<sup>2</sup>. For sand paper scratched wire (SW), the average CHF observed was 121.8 kW/m<sup>2</sup>, and an average CHF of 177.9 kW/m<sup>2</sup> was noted for the graphene oxide coated wire.

The critical heat flux value for a bare wire (BW) was considered as the base case for comparison against all the experiments conducted. No significant increase in CHF was observed for a sand paper scratched wire (SW) as compared against that of the bare wire. A significant increase of 50% was achieved for a graphene oxide -oated NiCr wire (GO50). The boiling curves for the three different heating surfaces up to the critical heat flux limit are shown in the Figure 4:2.

*Table 4-1 Experimental CHF values of bare wire, scratched wire and graphene oxide wire heaters*

	<b>BW</b> <b>(kW/m<sup>2</sup>)</b>	<b>SW</b> <b>(kW/m<sup>2</sup>)</b>	<b>GO50</b> <b>(kW/m<sup>2</sup>)</b>
<b>Trial 1</b>	118.4	117.3	180.0
<b>Trial 2</b>	120.3	123.6	177.1
<b>Trial 3</b>	119.3	128.5	177.5
<b>Trial 4</b>	117.4	117.9	177.5
<b>Trial 5</b>	117.4	121.7	177.5
<b>Average</b>	118.5	121.8	177.9
<b>CHF Enhancement</b>	N/A	2.8 %	50 %
<b>95% CI</b>	±1.11	±1.04	±1.79

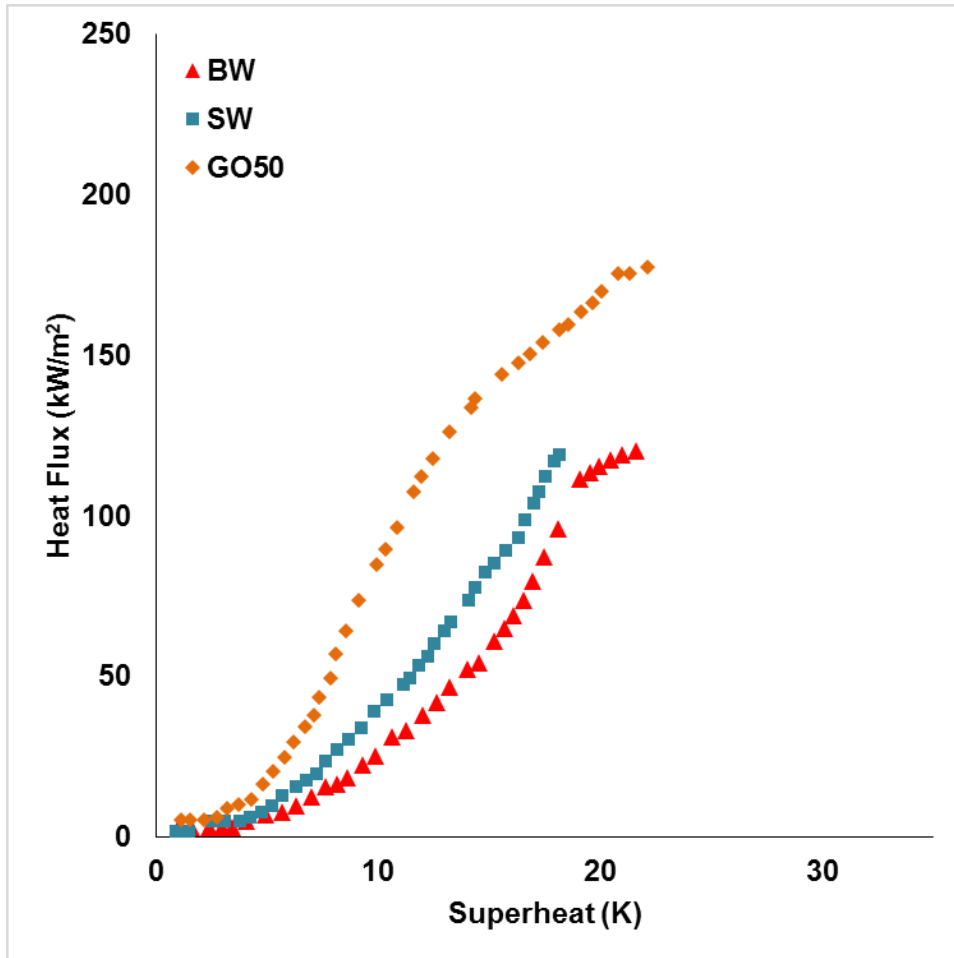


Figure 4:2 Pool Boiling curves for bare, scratched and graphene oxide coated wires

#### 4.1.2 Effect of Heater Surface on Hysteresis

The heating and cooling curves for a bare wire following the procedure discussed above are shown in the Figure 4:3. The data clearly suggests the evidence of hysteresis. With increase in heat flux,  $\Delta T$  increased up to  $\sim 12$  K beyond which increase in  $q''$  reduced  $\Delta T$ . During the cooling cycle, the curve traced a different path instead of following the heating curve. It was noted that when experiment was

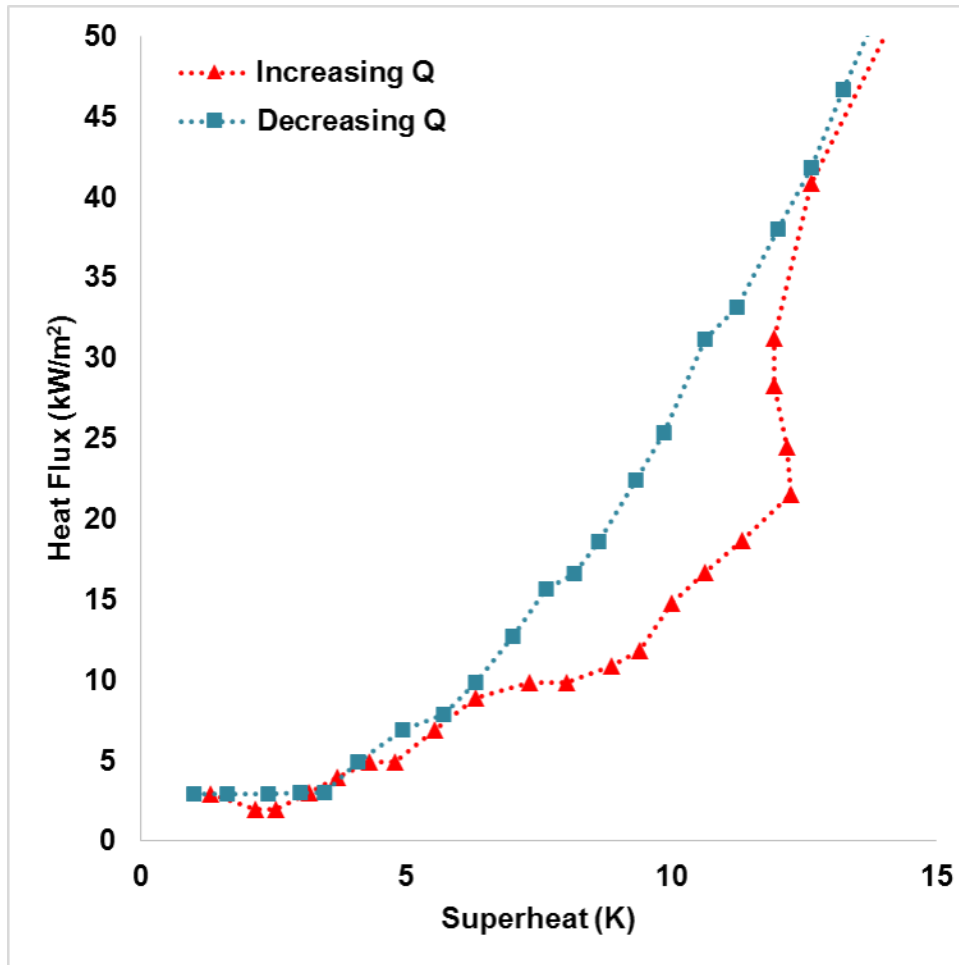


Figure 4:3 Hysteresis effect observed for FC-77 boiling on bare NiCr wire

repeated, the wire continued to show hysteresis effect, although at a reduced level. Typically after four to five runs, hysteresis effect completely vanished. The physical implication of this effect is that for a thermal system with surface finish similar to that of a bare wire under consideration, when operated below a heat flux of about 21.5 kW/m<sup>2</sup>,  $\Delta T$  will be higher, which in many applications may be unacceptable.

The heating and cooling curves for a scratched wire are shown in the Figure 4:4. There was no apparent difference between the cooling and heating curves of

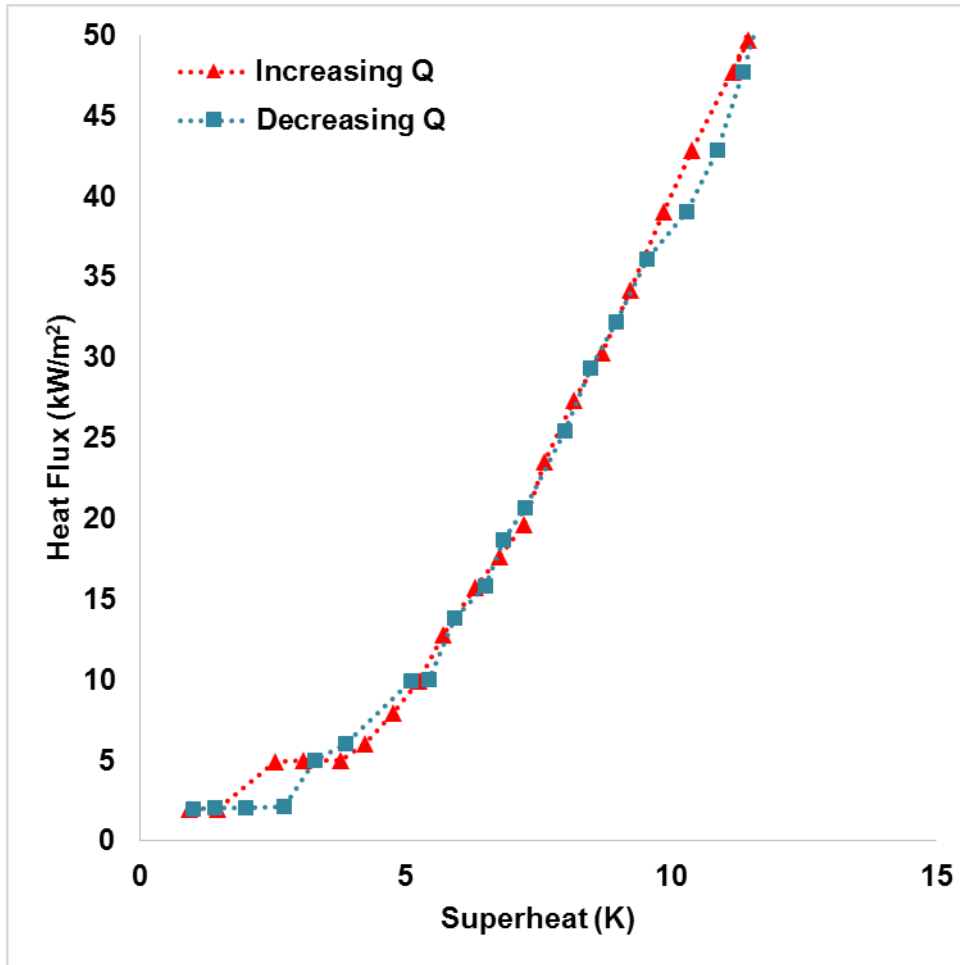


Figure 4:4 Heating and cooling curves for FC 770 boiling on scratched wire

the scratched wire. Although the highly wetting FC 770 floods the wire at low heat flux range, the roughness allows trapping of relatively more number of vapor embryos that act as nucleation sites and inhibit temperature overshoot from taking place. From the data, it is seen that the heating and cooling curves traced the same path indicating the absence of hysteresis.

The heating and cooling curves for a graphene oxide coated wire are shown in the Figure 4:5. As seen from the graph, there is no difference between the cooling

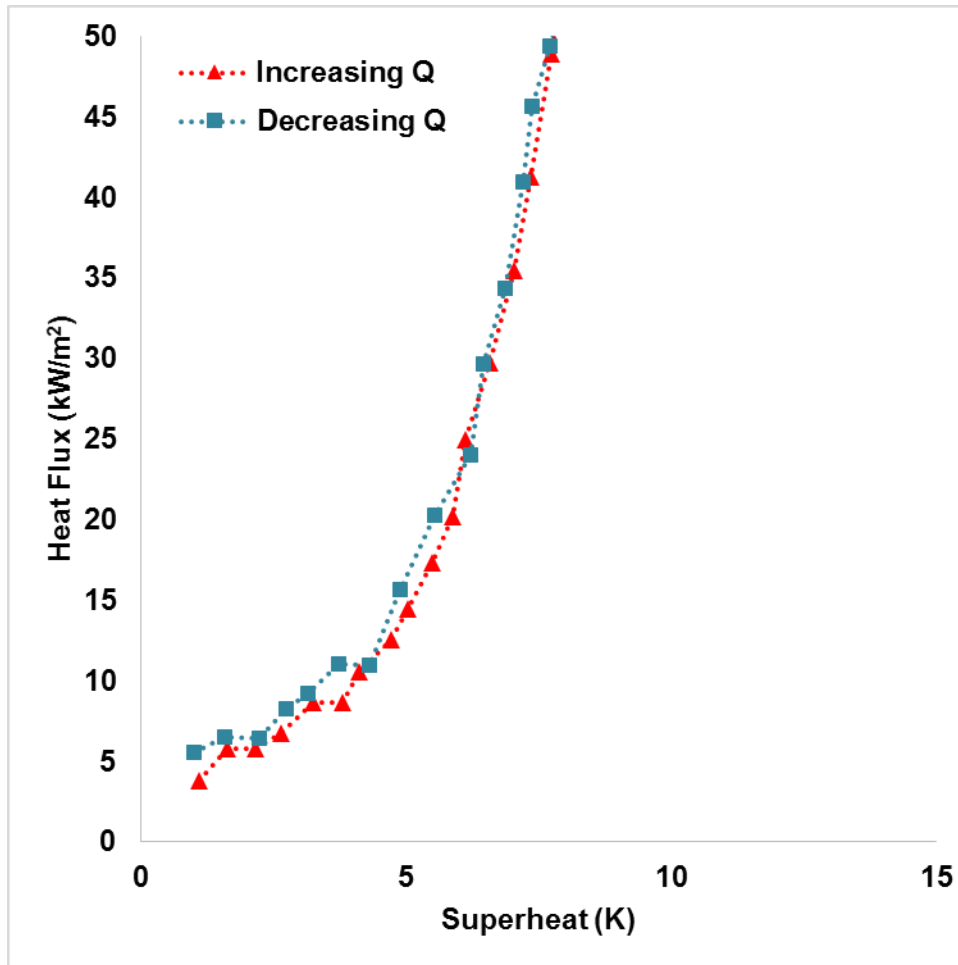


Figure 4:5 Heating and cooling curves for FC770 boiling on graphene oxide-coated wire

and heating curves, implying the absence of hysteresis effect for graphene oxide-coated sample. It can be explained by the increased roughness induced by the characteristically assembled rough layer of graphene oxide during dip-deposition. Despite flooding of FC 770 at lower heat flux values, the nano-scale vapors were expected to be trapped inside the nano-rough layers of graphene oxide that activated boiling nucleation sites. From the above results, it can be concluded that

graphene oxide coating provides safer operating conditions even at lower heat flux range and removes heat effectively from the heated surface. In electronics cooling applications, the chip can be allowed to be operated even at lower power densities, and still provide effective cooling. It can be concluded from the results that roughness controls hysteresis phenomena, and graphene oxide coatings prove to be an ideal surface for pool boiling.

## **4.2 Analysis of Boiling Curves for Various Heating Surfaces**

Many theories have been suggested to predict the CHF phenomenon such as hydrodynamic instability theory, macro-layer dry-out theory, hot/ dry spot theory and the bubble-interaction theory. One of the most popular theories to predict the CHF value is the Helmholtz instability [35] theory given by:

$$q_{CHF}'' = \frac{\pi}{24} \rho_l^{0.5} h_{fg} \sqrt[4]{g \sigma (\rho_l - \rho_g)}$$

where  $\rho_g$ ,  $h_{fg}$ ,  $\sigma$ ,  $g$  and  $\rho_l$  are respectively the vapor density, latent heat of vaporization, surface tension, acceleration due to gravity and liquid density of the working fluid. The CHF values observed in our experimental data for the bare and scratched wires are lower than the predicted CHF (reported in Table 4-1). This variation in predicted CHF and experimental CHF was also observed by Seo et al.[18] in their pool boiling experiments with a similar kind of fluorocarbon fluid namely FC 72. The difference was attributed to the different surface characteristics

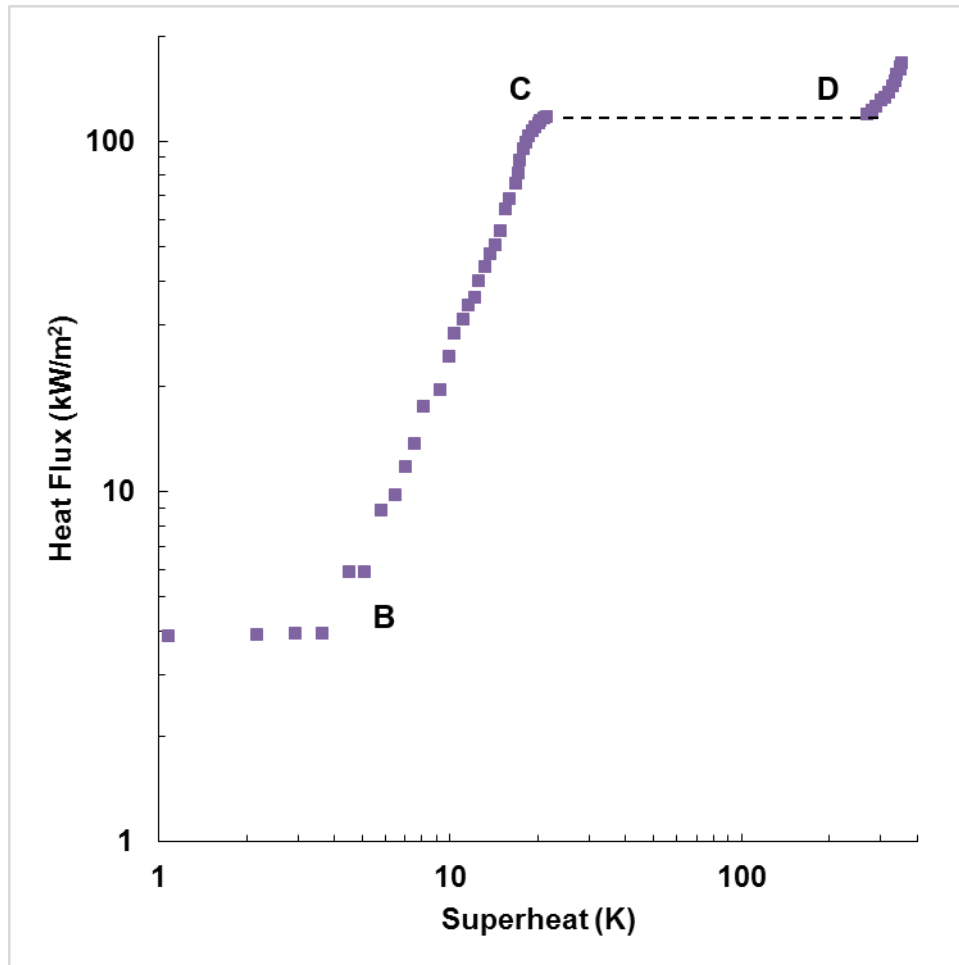


Figure 4:6 Boiling curve for bare nichrome wire showing free convection, nucleate boiling and film boiling regime

of the heater and other uncertainties such as wire orientation, wire to liquid-air interface distance and other random uncertainties that may occur.

After the disappearance of hysteresis for bare NiCr wire, the same set of heating wires were employed to obtain the complete pool boiling curves. The complete boiling curve for a bare NiCr wire (BW) is shown in the Figure 4:6. For a



given bare NiCr wire, at the present experimental conditions, the boiling crisis point or CHF occurred at an average value of  $118.5 \text{ kW/m}^2$  and the corresponding wall superheat was  $\Delta T = 21.8 \text{ K}$ . It was observed that the transition from free convection boiling to onset of nucleate boiling occurred at a wall superheat of  $\sim 7 \text{ K}$ , which was accompanied by initiation of bubble formations typically from surface defects. The heat flux corresponding to the onset of nucleate boiling point B was  $\sim 10 \text{ kW/m}^2$ . With increase in heat flux beyond point B on the graph, the number of nucleation sites increased the boiling more intense with concomitant increase in the heat transfer coefficient. At an average heat flux value of  $118.5 \text{ kW/m}^2$ , the boiling crisis point was reached and the wall superheat jumped from  $\sim 21 \text{ K}$  to  $\sim 300 \text{ K}$  denoted by the transition from point C to D on the boiling curve. Correspondingly, the heater temperature increased from a value of  $\sim 389 \text{ K}$  to  $\sim 668 \text{ K}$ . It is noted that the heater temperature after transition,  $\sim 668 \text{ K}$ , is still below the melting point of the wire, the working fluid may degrade. In addition, in many applications such as in electronics cooling, this temperature is higher than the acceptable limit for reliable operation of the device. By carefully controlling the input heat flux value, the boiling curve at the film boiling region was traced. At this stage, the convection from surface was greatly reduced and the heat transfer was predominantly due to conduction through the vapor and radiation from wire. Few

points plotted in the film boiling regime are also shown in the Figure 4:6. The

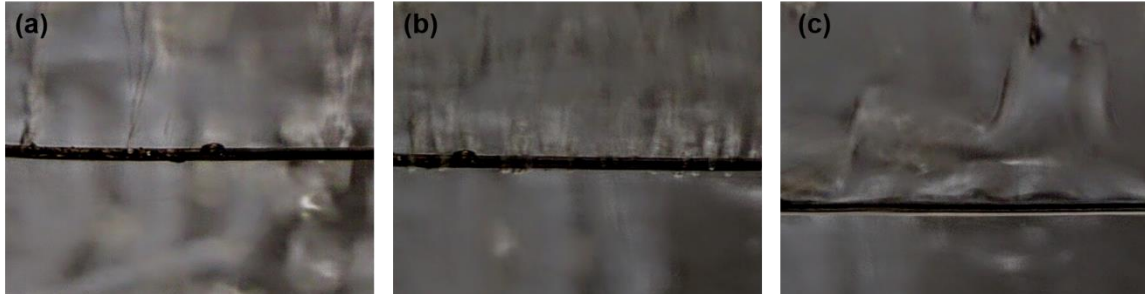


Figure 4:7 Visualization of pool boiling of FC770 on bare NiCr wire in (a) Free convection region, (b) Nucleate boiling region and (c) Film boiling region

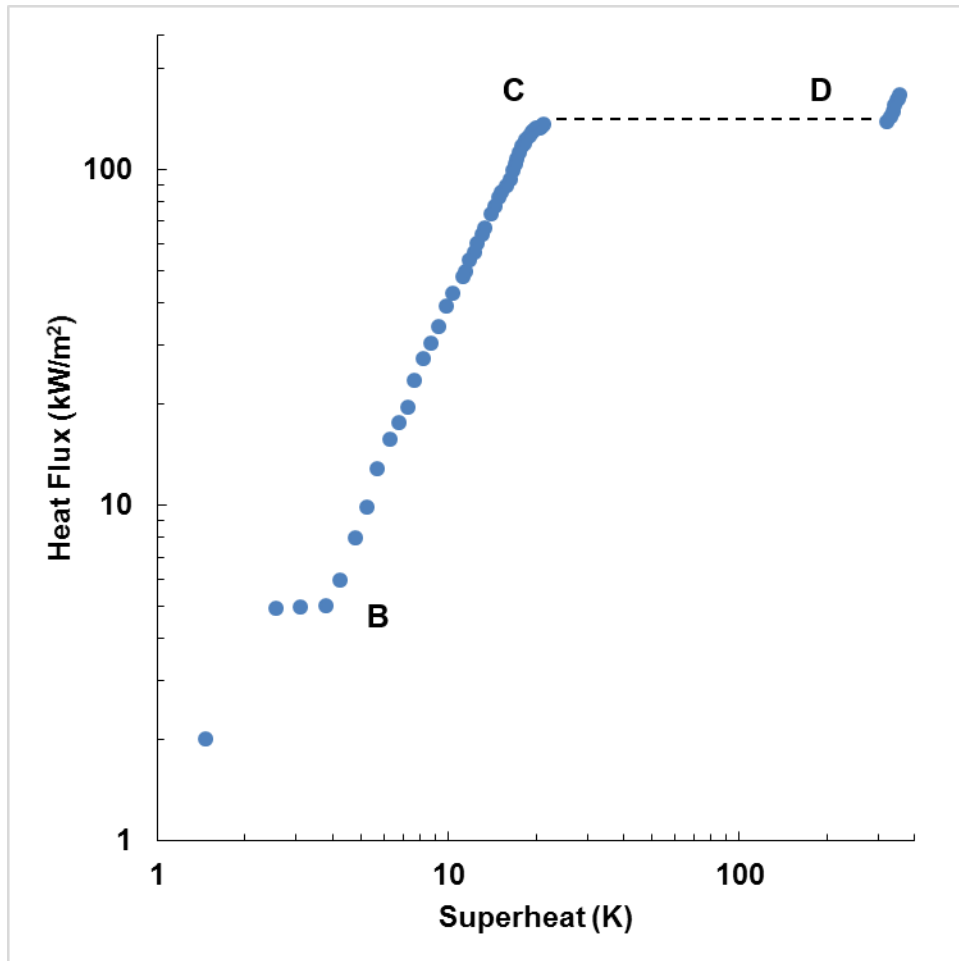


Figure 4:8 Boiling curve for scratched nichrome wire showing free convection, nucleate boiling and film boiling regime

pictures shown in the Figure 4:7 provides visualization of bubble formations at various regimes of boiling on a bare wire (BW).

The complete boiling curve for a scratched wire (SW) is shown in the Figure 4:8. For a scratched wire heater, the experimental critical heat flux point occurred at an average value of  $121.8 \text{ kW/m}^2$  with the corresponding wall superheat at  $\sim 21 \text{ K}$ . The transition from free convection boiling to nucleate boiling occurred at a wall superheat of  $\sim 5 \text{ K}$ . The heater temperature jumped from a value of  $\sim 389 \text{ K}$  to  $\sim 673 \text{ K}$  at the boiling crisis heat flux point indicating the operating limit. The main purpose of analyzing the boiling curve of a scratched wire was to compare the differences in effects produced by the roughness induced by sand paper-scratching and the self-assembled porous-rough surface of graphene oxide. It was also used to study the effect of roughness as a mechanism for critical heat flux enhancement, which will be explained in the later sections in this chapter. The data shows that hysteresis was eliminated because of the increased roughness but no significant variation in CHF was observed.

The complete boiling curve for a graphene oxide coated wire (GO50) is shown in the Figure 4:9. The boiling crisis point for a GO50 wire occurred at a heat flux of  $177.9 \text{ kW/m}^2$  and a wall superheat of  $\sim 22 \text{ K}$ . The transition from free convection boiling to nucleate boiling occurred at a heat flux of  $10 \text{ kW/m}^2$  and the corresponding wall superheat recorded was  $\sim 3 \text{ K}$ . At the boiling crisis point, the wire temperature jumped from  $\sim 390 \text{ K}$  to  $\sim 670 \text{ K}$  indicating a transition from

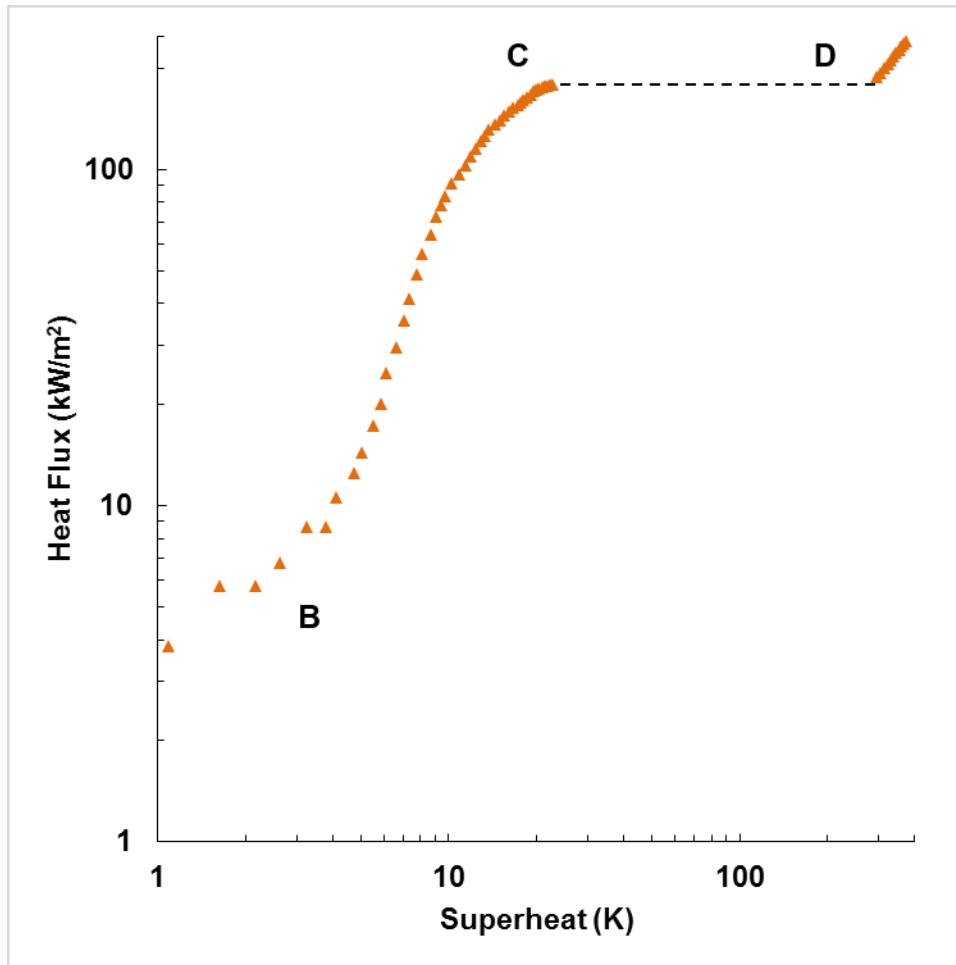
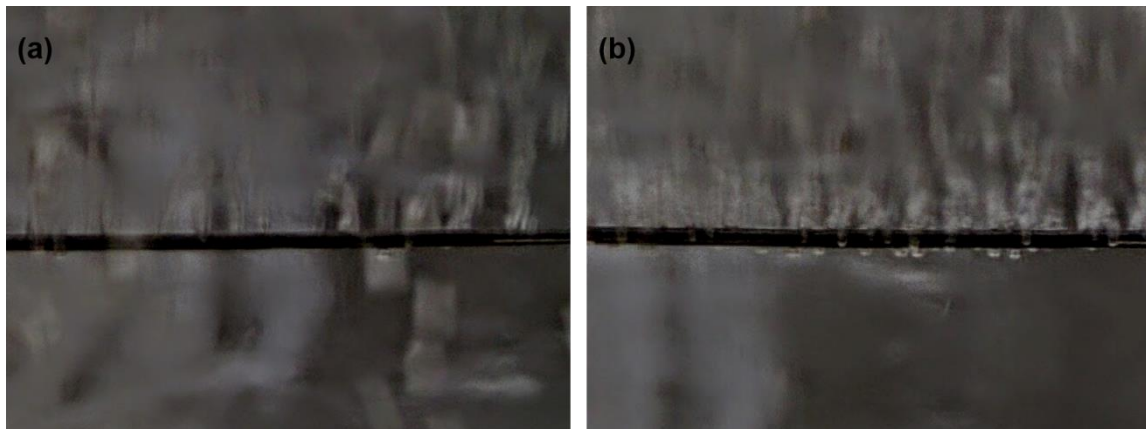


Figure 4:9 Boiling curve for graphene oxide-coated nichrome wire showing free convection, nucleate boiling and film boiling regime

nucleate boiling to film boiling regime. In practical applications, for heaters with surface characteristics similar to the GO50, the operating limit should be below a value of 177.9 kW/m<sup>2</sup>, which is about 50% higher than that for a bare NiCr wire. Thus, graphene oxide coating allows operations at higher power density levels. For thermal management of supercomputers, whose power densities are going up rapidly, graphene oxide layer can be potentially a good choice for surface coating.

Though supercomputers are cooled by flow boiling processes, which involves even higher heat transfer coefficients, pool boiling study serves as an ideal base case to understand the feasibility of present surface modifications using graphene oxide.

A summary of findings discussed above is as follows: the onset of nucleate boiling point for bare, scratched and graphene oxide-coated wires occurred at values of decreasing wall superheats ( $7\text{ K} > 5\text{ K} > 3\text{ K}$ ) and boiling crisis happened at values of increasing heat flux values ( $118.5\text{ kW/m}^2 > 121.8\text{ kW/m}^2 > 177.9\text{ kW/m}^2$ ). It can be concluded that the increased roughness of the surface shifts the incipient nucleate boiling point to lower superheat values. Due to the improved surface roughness, bubble nucleation was activated at lower wall superheat values. The greatest advantage of surface roughness is the existence of large number of nucleation sites, which promote growth and release of highly populated bubbles. The amount and rate of bubble generation for a rough surface was always higher



*Figure 4:10 Visualization of nucleation site density for the same heat flux of  $90\text{ kW/m}^2$  (a) Bare wire and (b) Graphene oxide-coated wire. The number of active nucleation site density for graphene oxide coated wire is observed to be significantly higher than that for a bare wire*

when compared to that for a bare polished surface. It can be clearly shown by comparing the photographs of bubble formation at the same input heat flux of 90 kW/m<sup>2</sup> for a bare and graphene oxide-coated wires (Figure 4:10). As the enhanced roughness in scratched wire did not cause a substantial CHF enhancement, the governing parameter for the increased CHF value for graphene oxide coating could not be determined only by considering roughness as the affecting factor. To address this problem, a comprehensive parametric sensitivity analysis is performed and is discussed in the section 4.3

### **4.3 Mechanisms of CHF and BHT Enhancement**

As discussed in section 1.3, critical heat flux (CHF) and boiling heat transfer (BHT) enhancement mechanisms have been widely studied to determine how the critical heat flux varies with alterations in the surface characteristics induced by graphene oxide coatings. The CHF limit is primarily dependent on the properties of the working fluid and heating surface. The surface parameters that can possibly affect the CHF enhancements are wettability, surface roughness, porosity and thermal activity. In past research undertaken in pool boiling on graphene oxide deposited surfaces, the CHF enhancement mechanisms were attributed to the parameters as shown in Figure 1:4.

### 4.3.1 Effect of Wettability

Wettability of the surface or working fluid plays a vital role in CHF enhancement, especially at the region closer to boiling crisis point [36]. A highly wetting fluid or a surface aids in efficient rewetting of the surface at high heat flux region, and thus delays the occurrence of boiling crisis by shifting the critical heat flux to a higher value. There has been a number of investigations, which measured the apparent contact angle to quantify wettability and study its effect on CHF enhancement. Values of the measured contact angle of FC 770 droplet on different heating surfaces are shown in the Figure 4:11. The contact angle subtended on a bare wire was  $24^\circ$ ; on the scratched wire  $26^\circ$ , and on the graphene oxide coated surface was  $23^\circ$ . It can be seen that the contact angle does not vary substantially for any of the surfaces considered. This can be attributed to the very low surface tension of FC 770 ( $0.015 \text{ N/m}$ ) when compared to that of water ( $0.06 \text{ N/m}$ ). It is reasonable to conclude that wettability does not play a role in the observed enhancement for CHF.

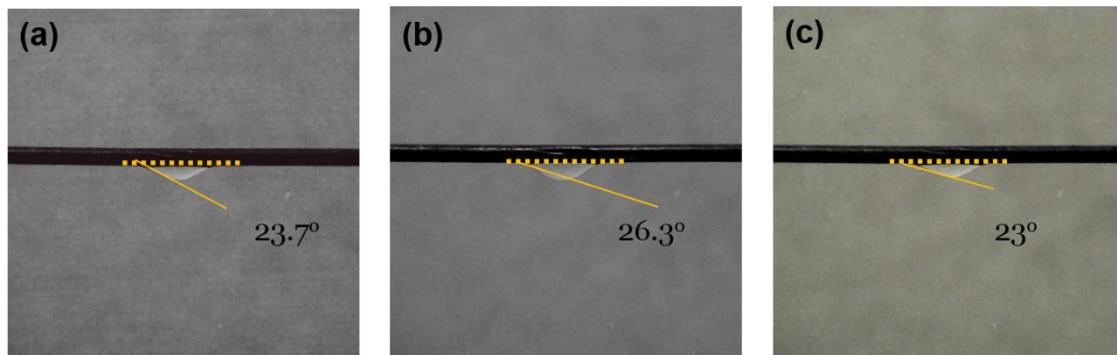


Figure 4:11 Apparent contact angle of FC 770 on (a) bare wire, (b) scratched wire and (c) graphene oxide-coated wire.

### 4.3.2 Effect of Surface Roughness

Roughening the working surface using sand papers or abrasives is one of the earliest techniques followed to modify the surface morphology to improve boiling heat transfer performance. Kurihara et al. [37] investigated the pool boiling phenomena on roughened flat surfaces and found that the number of active boiling centers enhanced the nucleate boiling performance. The increased number of active boiling centers or nucleation sites may augment the heat transfer coefficient

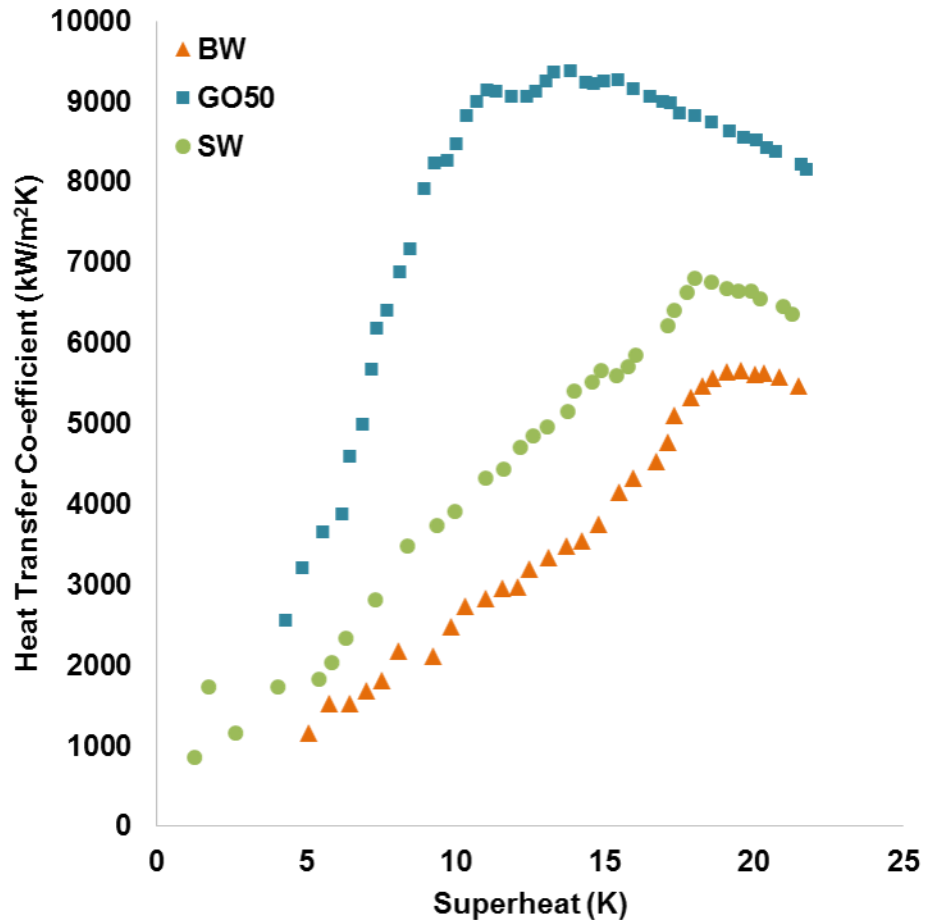


Figure 4:12 Effect of surface roughness on nucleate boiling heat transfer



through increased bubble generation and agitation. Effect of surface roughness on critical heat flux is not well known. Some of the researchers [38], [39] showed that CHF is independent of surface roughness and that it is responsible only for the enhanced heat transfer coefficient. For a liquid with high surface tension like water, the increased surface roughness may have some effect on the CHF as it may alter the wettability. However, for FC 770, it is seen that roughness did not have any influence on wettability. It was also seen that there was no significant increase in CHF for a sand paper scratched wire, as compared against smooth bare wire, in spite of the increased surface roughness. It follows, therefore, the CHF enhancement mechanism observed for graphene oxide-coated wires may be partially attributed to the surface roughness.

The heat transfer coefficients for bare wire, scratched and graphene oxide coated wires are shown in the Figure 4:12. The data presented in the graph were obtained by decreasing the heat flux to avoid the hysteresis effect that may occur during the heating cycles of bare wires. The obtained data indicates that surface roughness significantly enhances the boiling heat transfer performance. In summary, surface roughness eliminates hysteresis, augments BHT coefficient but does not influence on the CHF limit.

### 4.3.3 Effect of Porosity

An objective of the thesis work was to investigate critical heat flux enhancement mechanism associated with pool boiling of FC 770 on porous graphene oxide layer coating. Since the development of porous metallic coatings, they have received much attention among researchers for studying the effect of porosity on pool boiling phenomena [32]. Porous metallic coatings were generally formed on a plain surface by bonding small metal particles to it at various thickness levels. These coatings have been shown to substantially amplify the nucleate boiling heat transfer coefficient because of the increased nucleation site density and enhanced working fluid transport between these sites. Within a porous media, it is expected that the evaporation rate of thin film of liquid will be higher with increased effective surface area, which accounts for BHT augmentation. Previous

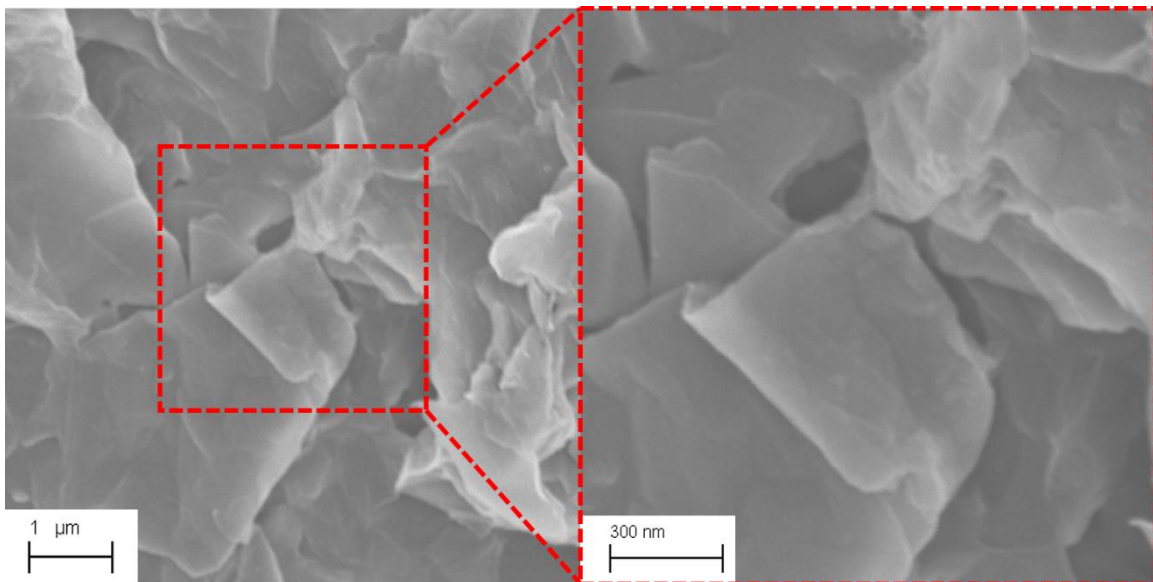
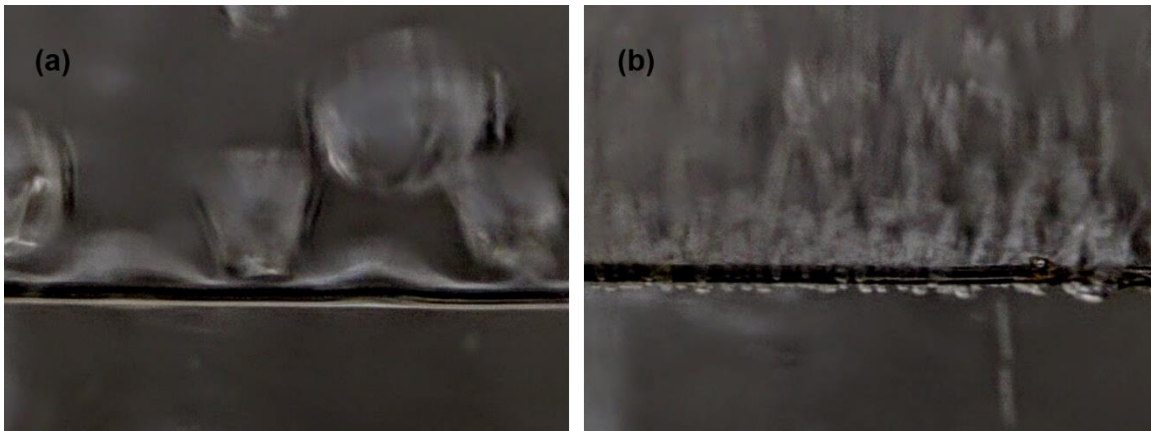


Figure 4:13 SEM Image of porous graphene oxide coating on NiCr wire

research in this area had shown that microporous coatings also significantly enhanced the critical heat flux of highly wetting fluids [40].

For observing the surface morphology, a SEM image of graphene oxide coating on NiCr wire is shown in Figure 4:13. It can be seen from the image that the graphene oxide layer consists of flakes and regions of large-sized pores between the flakes. In addition to the micro-sized pores, each flake contains nano-pores or cavities as depicted in the enlarged image in Figure 4:13. Permeability, which is one of the characteristics of a porous structure, allows liquids or vapors of working fluid to flow through. Thus, permeability helps in quantifying the liquid or vapor flow conductance in a porous media. In any porous structure with high permeability, it enables new liquid to enter into the structure and causes the vapor to escape out of the porous layer. In other words, the new liquid entering the porous structure inhibits the formation of large vapor bubbles, which diminish the heat transfer performance. The nano-pores or cavities on the graphene oxide flakes act as nucleation sites for vapor generation, and the micro-pores between flakes promote penetration of liquid into the structure and aid in flow of vapor out of the porous layer. Thus, the self-assembled porous structure of graphene oxide improves the migration of vapor bubbles, and the liquid penetrated into the structure resists the formation of vapor blanket, which may cause significant decrease in CHF and BHT performance.

Absence of porosity for bare and scratched nichrome wires, is a contributing factor to the lower critical heat flux values for the bare and scratched wires. This explains the lower critical heat flux values for bare and scratched wires. Figure 4:14 shows the photographs taken at the heat flux region closer to critical heat flux for bare and graphene oxide-coated wires. It is observed that the number of active nucleation sites for graphene oxide is significantly higher than for bare wire. At high heat flux region, due to the lack of highly populated nucleation sites in a plain surface, the vapor bubbles grow in size before leaving the surface. As the bubbles grow in size, they coalesce to form pockets of vapor blankets on the heater. The heat transfer mode is primarily by conduction through the vapor layer, and is relatively much weaker than by nucleate boiling. For a graphene oxide-coated surface, it is observed that the nucleation site density is still large as a result of the high porosity and permeability of the graphene oxide layer, which permit the flow



*Figure 4:14 Photographs taken at 90% of CHF for (a) bare wire and (b) graphene oxide coated wire. The picture clearly depicts the highly populated nucleation sites for a porous graphene oxide layer as compared against a bare NiCr wire.*

of liquid and vapor through the micro-pores. Thus, boiling heat transfer mechanism for a graphene oxide coated wire can be explained by both forced convection and latent heat transfer at high heat flux regions.

Polezhaev and Kovalev [41] modeled boiling heat transfer process on porous surfaces. They observed that the enhancement in critical heat flux was due to decreased vapor jet spacing and increased vapor jet velocity, which is in agreement with the results obtained in the current research undertaken. They derived the following model for predicting CHF on porous surfaces:

$$q_{CHF}'' = 0.052 \varepsilon^{2.28} h_{fg} \frac{\sigma \rho_l \rho_g}{(\rho_l + \rho_g) r_p}$$

where  $\varepsilon$  is the porosity,  $h_{fg}$  is the latent heat of evaporation of working fluid,  $\sigma$  is the surface tension,  $\rho_l$  is the density of liquid,  $\rho_g$  is the vapor density and  $r_p$  is the pore radius. Liter and Kaviany [42] also modeled boiling on porous surface to predict the critical heat flux. They took permeability of porous surface into account and explained CHF in terms of capillary limit. The following model was derived by creating balance between capillary pumping force and liquid viscous drag along the flow path:

$$\frac{q_{CHF}''}{0.53 \left( \frac{\rho_l \sigma h_{fg}}{\mu_l} \right) (K\varepsilon)^{0.5} / D} = 1 - \frac{C_E}{0.53} \frac{D}{\varepsilon^{0.5}} \frac{q_{CHF}''^2}{\rho_l \sigma h_{fg}^2}$$

$$C_E = \left( \frac{0.018}{\varepsilon} \right)^{0.5}$$

where  $\mu$  is the viscosity of the liquid,  $K$  is permeability of the wicking porous structure,  $C_E$  is the Ergun coefficient,  $D$  is the liquid flow distance and  $\varepsilon$  is the porosity. Based on the SEM images, it is observed that the porosity and permeability of graphene oxide layer used in the present study are significant and the characteristics of graphene oxide layer are quite similar to the porous graphene

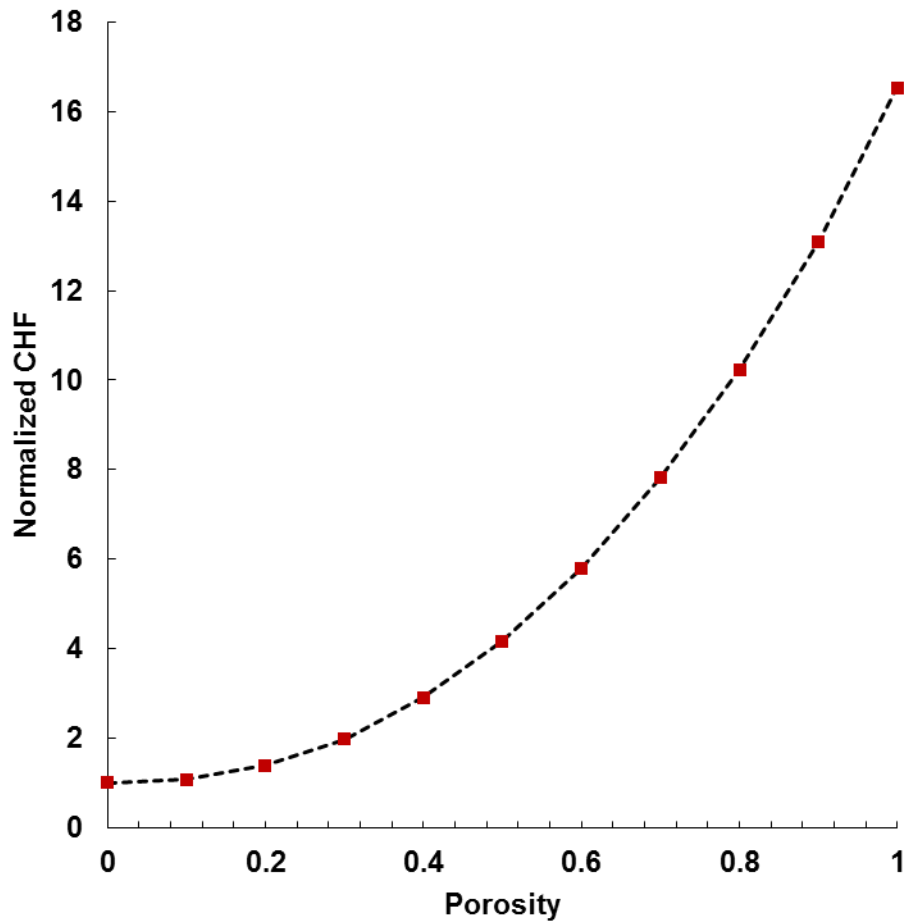


Figure 4:15 Sensitivity of porosity with predicted CHF (Polezhaev and Kovalev [41])

layer used by Seo et al. [18]. Since the graphene oxide was synthesized chemically using a process very similar to that used by Seo et al., we used the the values of

porosity and permeability reported for graphene oxide by them. Using these values, the predicted value of critical heat flux using Polezhaev and Kovalev's model was  $145.6 \text{ kW/m}^2$ , which is 1.15 times the CHF for a bare wire. The predicted CHF values using the Liter and Kaviany's model for a permeability value of  $2.01 \times 10^{-10} \text{ m}^2$  was  $351.2 \text{ kW/m}^2$ , which is about 277 % higher than the base value for bare wire. The CHF values predicted from these models don't match the experimental

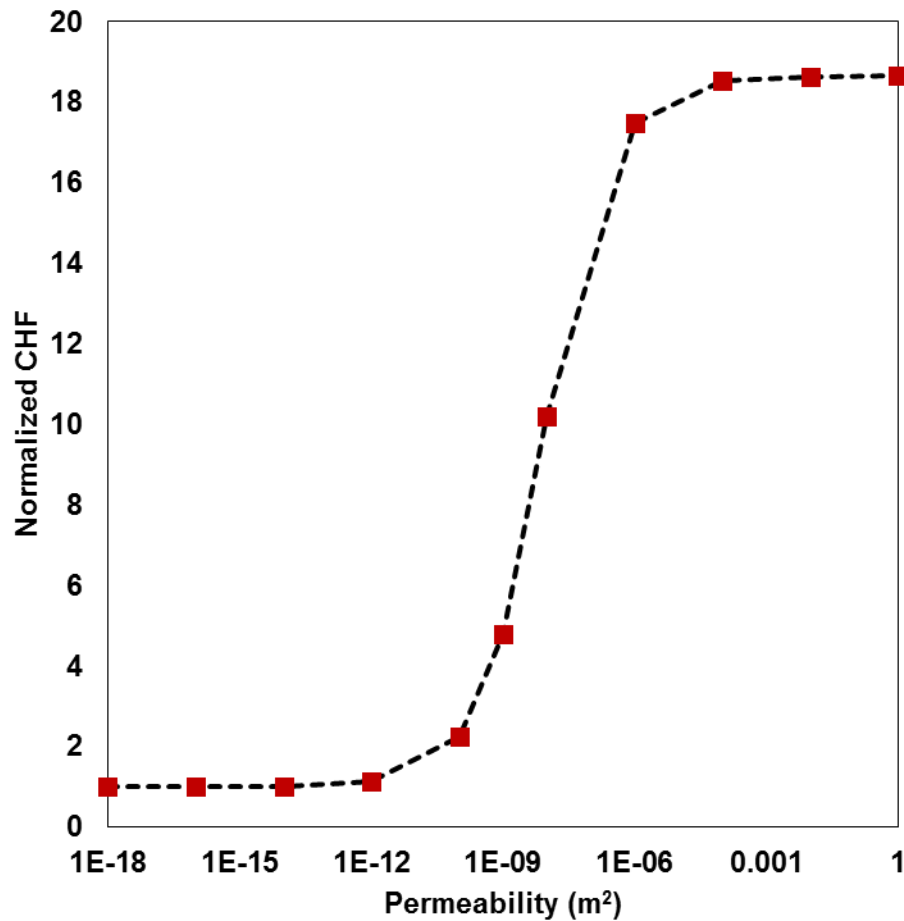


Figure 4:16 Sensitivity of permeability with predicted CHF (Liter and Kaviany [42])

results in the present study, possibly because the model is valid only under the original experimental conditions used. However, the above models suggest an idea of contribution of porosity and permeability to the enhanced CHF observed in the present study. To get an idea of the effect of permeability on CHF, calculations were made for different values of permeability. These are plotted in Figure 4:16. It is seen that there is an exponential rise in the CHF from values of permeability from  $1 \times 10^{-12}$  to  $1 \times 10^{-8}$  m<sup>2</sup>. From the above analysis, it can be concluded that the CHF enhancement mechanism can be clearly explained in terms of porosity of the deposited layer.

#### **4.3.4 Effect of Thermal Activity**

Watwe and Bar-Cohen [43] developed a model for studying the effects of heat conduction on pool boiling CHF enhancements for dielectric fluids. As discussed earlier in section 4.2, the nucleation sites could be distributed randomly on the heating surface. At locations where the density of nucleation sites is low, it leads to the formation of local vapor mushrooms, by coalescence of vapor bubbles or columns in the lateral direction. The liquid lying underneath the vapor mushroom soon depletes and creates local hot spots whose temperature increases significantly due to the applied heat flux. The rise in temperature can be tolerated by the ability of the material to absorb heat, and spread the temperature effectively to the adjacent nucleation sites. As defined in section 1.1, *Leidenfrost* temperature is the temperature at which the rewetting of the surface becomes impossible. If the



temperature of the local spot at the end of the residence time of the vapor mushroom goes beyond the *Leidenfrost* point, quenching of the surface by rewetting of working liquid is inhibited. This leads to the evolution of local dry spot into global dry out, and the boiling crisis occurs. In case of a thin heater with low thermal properties, CHF occurs immediately after first local dry spot is created on the heater surface. Thus, CHF is dependent on the thermal properties of the wire that aids in effectively spreading out the heat across the heater surface. The ability of the heater to conduct heat across the heater can be explained in terms of effusivity (E) and thermal activity (S) of the heater material [44]. Effusivity quantifies the ability of a material to absorb heat, and is a property of the material. Thermal activity is the product of characteristic thickness of the heater and its effusivity.

$$E = \sqrt{\rho_h C_h K_h}$$

$$S = t_h \sqrt{\rho_h C_h K_h}$$

where  $\rho_h$ ,  $C_h$ ,  $K_h$  and  $t_h$  are density, specific heat capacity, thermal conductivity and thickness, in that order, of the heater material. Experimentally it is determined that it is inappropriate to directly correlate the CHF enhancement mechanism to the thermal conductivity or effusivity of the material. As reported by Seo et al. [18], a pristine graphene layer of highest thermal conductivity of 5000 W/mK, enhanced the CHF just by about 8 %, whereas the thicker porous surface of graphene oxide of comparatively lower thermal conductivity or effusivity enhanced

the critical heat flux by about 89 %. Hence, CHF enhancement mechanism is explained in terms of thermal activity, which is a product of thickness and effusivity.

To consider a cylindrical wire as a flat plate heater, characteristic length, which is the half of wire diameter was considered. The characteristic length is assumed to be the heat exit path length across which the heat transfer by lateral conduction takes place. Since the cylindrical heater is considered as a flat plate heater in this method, the thermal activity of the thin film of graphene oxide can be directly added to that of plain wire heater. Bar-Cohen et al. [44] studied the effects of thermal conduction across the heaters using thermal activity analysis, and found that the following relation was valid for any heater material with a broad range of thermal activity (S can lie in the range 0.1 to 25):

$$\frac{q_{CHF}''}{q_{CHF,max}''} \propto \frac{S}{S + 0.8}$$

where  $q_{CHF,max}''$  is the asymptotic value of CHF used as a reference. Asymptotic CHF value is the maximum thermal limit for a particular type of heater, determined based on the thermal management abilities of the material, which depends on heater material properties and thickness. Bar-cohen et al. [44] found that 90% maximum CHF was obtained at a thermal activity of 8, and at  $S = 85$ , 99% of asymptotic CHF was approached. In the present study, the heater material used is a hybrid kind, comprising of graphene oxide film on NiCr wire. It is expected that

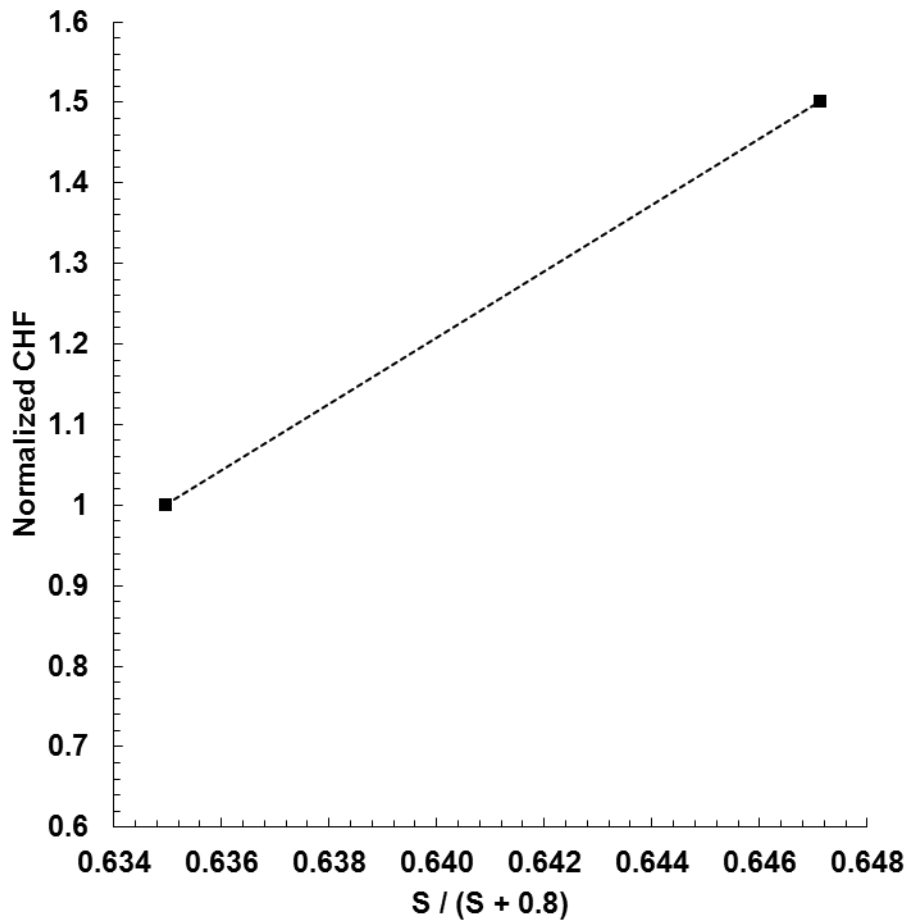


Figure 4:17 CHF as a function of thermal activity of the heating material

the value of asymptotic CHF varies with the type of heat used, and no research have been conducted on estimating the maximum CHF for hybrid materials. Since, there is a transition of material from poor thermal conducting wire to a wire with highly thermal conducting material, drastic changes in the asymptotic values and hence in the CHF may be observed. Based on the known values from material properties, the thermal activities for bare NiCr wire and graphene oxide coated wire, were estimated to be 1.3915 and 1.4671 respectively. Figure 4:17 shows the plot of normalized CHF against the  $S / (S + 0.8)$  ratio. It is also noted from the reference [44] that there was a momentous rise in the CHF with very small increase in thermal activity. Therefore, it is expected that there will be a steep rise in asymptotic CHF with an increase in thermal activity from 1.39 to 1.46. The current trend is also consistent with the results obtained in the reference [16] where the CHF enhanced about 75 % for a jump of thermal activity from 0.33 to 0.34. It can be concluded that the increase in CHF was caused by the steep rise in the thermal property of the thin film, which altered the asymptotic CHF to a higher value. In physical sense, a material with high thermal conductivity is expected to dissipate heat from local hot spots more effectively in lateral direction, and delays the occurrence of boiling crisis.

#### **4.4 Partial Reduction of Graphene Oxide**

Díez-Betriu et al. [45] studied the mechanism of chemical and thermal reduction of graphene oxide using Raman Spectrum characterizations. They

carried out thermal annealing of graphene oxide in the presence of inert nitrogen/argon atmosphere at temperatures below 300° C for 1 h to a total of 7 h. FC 770 is an inert fluid and it is expected that partial reduction of graphene oxide will occur

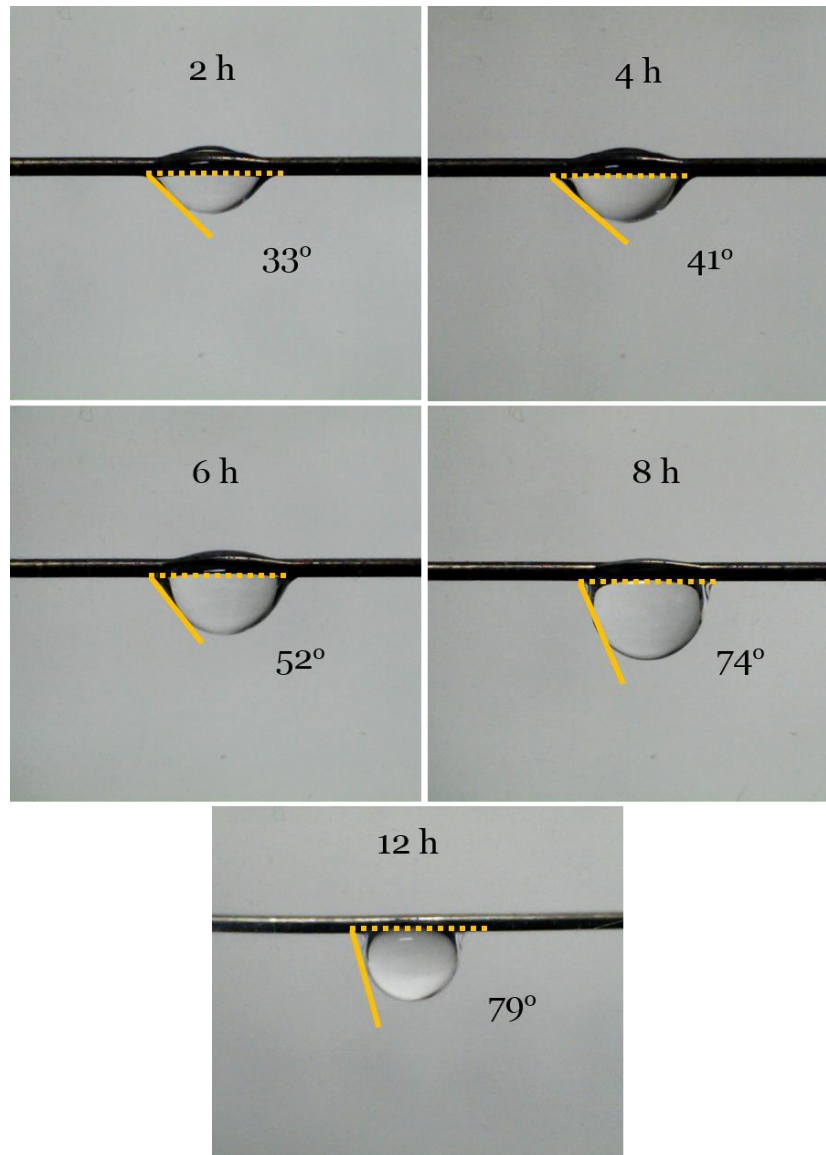


*Figure 4:18 Contact angle of water droplet on graphene oxide-coated wires at various nucleate boiling dwell times. There is a significant increase in contact angle showing that the surface is tending towards hydrophobicity, a characteristic property of pristine graphene.*

as the wall temperature goes beyond 100°C during the pool boiling. The extent of reduction depends on the exposure time of graphene oxide-coated surface to the high temperature environment. To test this hypothesis, a newly coated graphene oxide wire was exposed to a constant heat flux of  $\sim 150 \text{ kW/m}^2$  for various times (2 h, 2 h + 2 h, 4 h + 2h, 6 h + 2 h and 10 h + 2 h), and apparent contact angle measurements were taken at each stage. The apparent contact angle of water on the wire at different stages of reduction is shown in Figure 4:18. It is seen that there

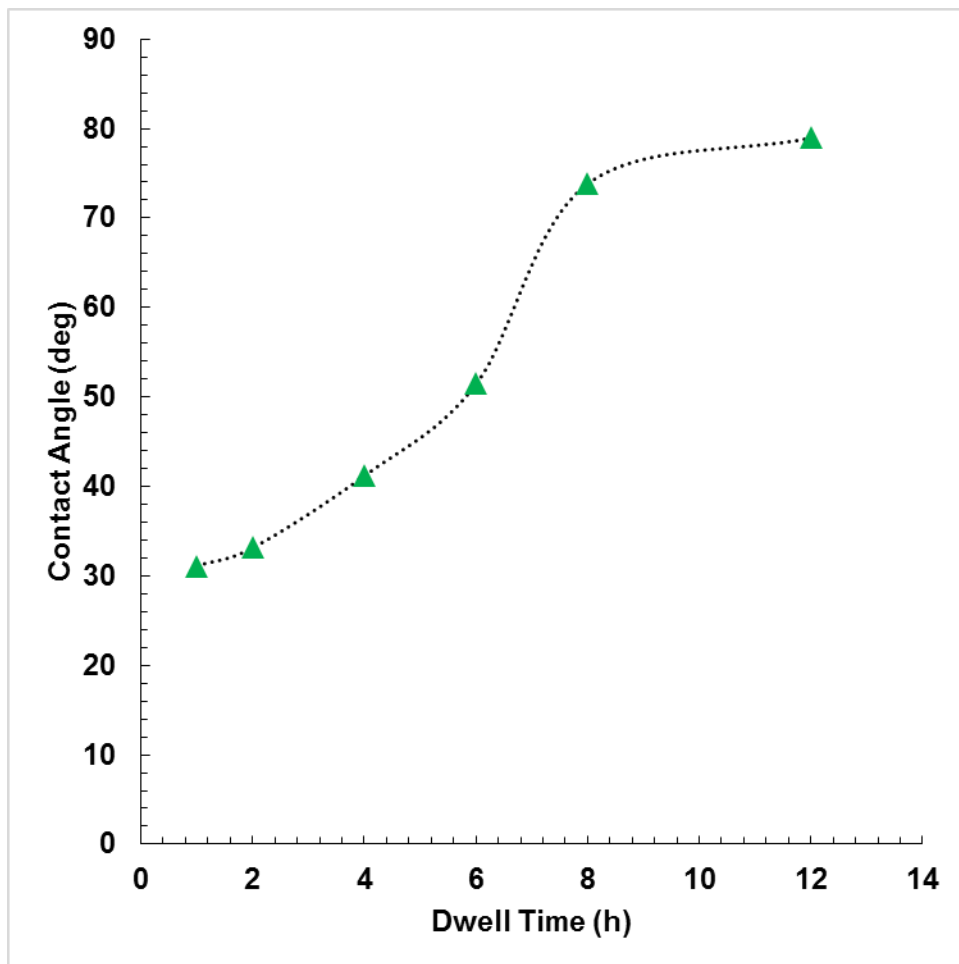


Figure 4:19 Contact angle as a function of nucleate boiling dwell time

is a prominent drop in the wettability of surface with increase in dwell time. A plot of contact angle against dwell time is shown in Figure 4:19. As the dwell time increased, the surface turned more hydrophobic, a characteristic property of pristine graphene, which suggests the partial reduction of graphene oxide. Thermal annealing of graphene oxide layer takes place during the nucleate boiling dwell time and promotes partial reduction process. A layer of as-synthesized graphene oxide contains non-uniform distribution of characteristic defects, hydroxyl groups (C – OH), epoxy (C –O- C), carbonyl (C=O) and carboxylic (-COOH) groups. The presence of carboxylic and other oxygen functional groups reduces the surface tension of liquid. This explains the hydrophilic nature of

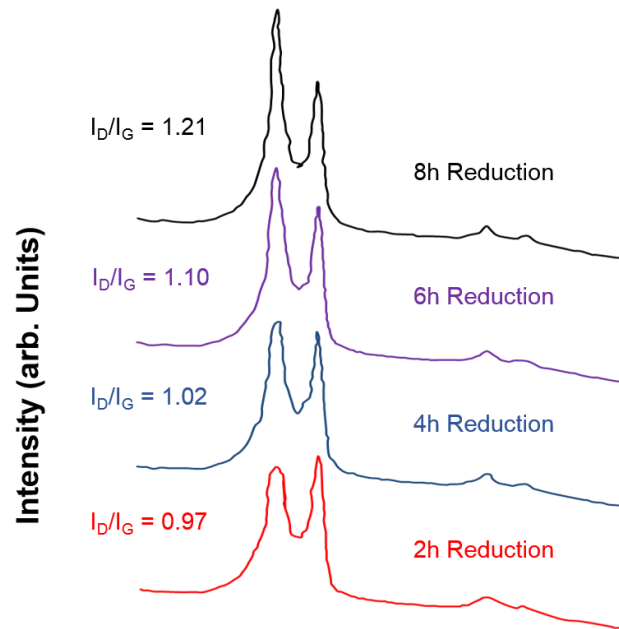


Figure 4:20 Raman spectrum of graphene oxide coating taken at different dwell times. There is a gradual increase in the  $I_D/I_G$  intensity ratio indicating the increase in surface defects.

graphene oxide. The apparent contact angle of water measured on a newly coated NiCr wire was observed to be 31°.

The wettability of graphene oxide is a function of coating thickness as reported by Park et al [17], and the contact angle corresponding to the present coating thickness may not be sufficiently high to make the surface superhydrophilic. At temperatures below 200°C, embedded water molecules, carboxylic

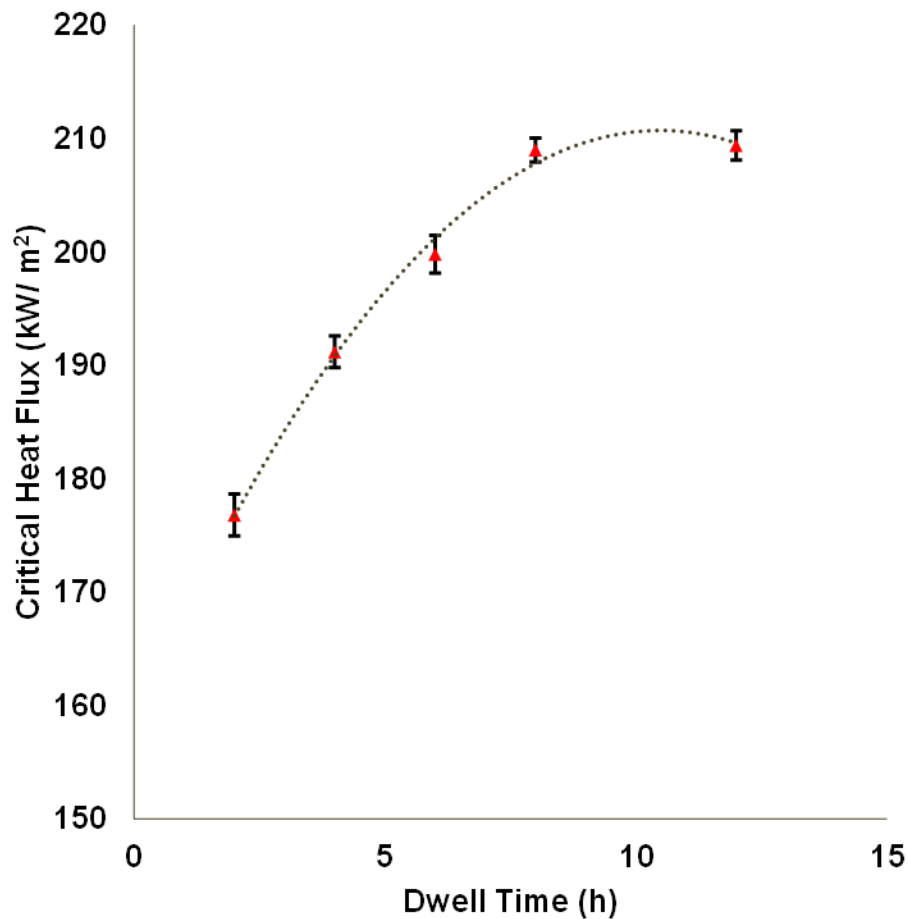


Figure 4:21 CHF as a function of nucleate boiling dwell time. There is an increase in CHF with increasing operation time of the heater.



groups and in-plane oxygen functional groups are eliminated [45]. The removal of oxygen functional group from a sheet of graphene oxide creates a hole, and augments characteristic surface defects. This results in an increase in characteristics defects with increasing reduction time. The change in defects density can be quantified using ID/IG intensity ratio in Raman spectrum (see Figure 4:20). The intensity ratio increases gradually from 0.97 at 2 h to 1.21 at 8 h, which clearly shows an increase in characteristic defects that was caused by the removal of oxygen functional groups from the graphene layer. As the carboxylic groups and other oxygen functional groups are removed, the thermal conductivity and number of active nano-cavities on graphene oxide sheet augment, and hence an increase in CHF with reduction is expected. To test this hypothesis, experiments were conducted on a newly coated wire, and CHF at each nucleate boiling dwell time was recorded. At each stage of reduction, the wire was taken to the CHF point and the average heat flux value was noted. Figure 4:21 shows the variation of CHF with nucleate boiling dwell time. As expected, there was an increase in critical heat flux, which saturated at a value of 209 kW/m<sup>2</sup>, which is about 77 % more than CHF for a bare NiCr wire. In a nutshell, partial reduction of graphene oxide was captured as the experiment continued, and a further enhancement in CHF of about 77 % was observed.

## Chapter 5

### 5 Conclusion

In this study, pool boiling experiments were conducted on bare, sand paper scratched- and graphene oxide-coated NiCr wires, using saturated FC 770 Fluorinert fluid. Graphene oxide was synthesized using a chemical method and dip-deposited on the NiCr wires to form a self-assembled porous, and micro-nano rough surface. The heater surface parameters such as wettability, surface roughness, porosity and thermal activity were examined to study the nucleate boiling heat transfer and critical heat flux enhancement mechanisms. The following conclusions were obtained.

- (1) The average critical heat flux values of bare wire, scratched wire and graphene oxide-coated wire respectively were  $118.5 \text{ kW/m}^2$ ,  $121.8 \text{ kW/m}^2$  and  $177.9 \text{ kW/m}^2$ .
- (2) No significant enhancement in the CHF of scratched wire was observed (2.8%), whereas an enhancement in CHF of about 50% was observed for graphene oxide coated wires.
- (3) Boiling curve hysteresis was evident for new bare wires that caused a temperature overshoot of up to 12 K during the first few runs. There was no difference between the heating and cooling curves of graphene oxide-coated wires, which indicated an absence of hysteresis effect. The increased surface

roughness of graphene oxide layer augmented the number of nucleation site densities and hence promoted bubble nucleation at lower superheat values.

(4) Since FC 770, a highly wetting fluid, subtended similar apparent contact angles on all the heating surfaces, CHF or BHT enhancement mechanisms could not be explained in terms of wettability of the fluid or heater surface.

(5) Roughness of the heater surface was found to improve the nucleate boiling heat transfer but had no effect on CHF enhancement mechanism.

(6) SEM and AFM characterizations revealed a highly porous layer of graphene oxide deposition, which had intercalating space between flakes, nano-pores on each flake and micro-pores between the flakes. Hence, CHF enhancement was explained in terms of porosity and permeability of the porous graphene oxide layer.

(7) CHF enhancement was also explained in terms of thermal activity, which is a function of heater thickness and effusivity. Highly thermal conductive graphene oxide coating shifted the asymptotic value of CHF to a significantly higher value, which further enhanced the CHF by acting as an effective heat spreader.

(8) Partial reduction of graphene oxide occurred during the nucleate boiling region, confirmed by water contact angle measurements and the Raman spectroscopy characterization at each stage of reduction. A maximum CHF

enhancement of about 77% was obtained, which saturated after 12 hours of operation of heater.

The results obtained served as a basis for studying the feasibility of using graphene oxide coatings for electronics and super computer cooling technologies.

***Suggestions for future work:***

- Study the pool boiling phenomena on GO/rGO-patterned surfaces and formulate a new model for pool boiling from such surfaces.
- Conduct pool boiling experiments for graphene oxide-coated metallic foams.
- Studying film- and drop-wise condensation on GO or rGO coatings.
- Develop a technique to form porous graphene oxide foams using GO coatings and phase change materials. Investigate performance of these foams for thermal management.

## Bibliography

- [1] A. Bar-Cohen, "Thermal Management of Electronic Components with Dielectric Liquids.," *JSME Int. J. Ser. B Fluids Therm. Eng.*, vol. 36, no. 1, pp. 1–25, 1993.
- [2] S. M. You, J. H. Kim, and K. H. Kim, "Effect of nanoparticles on critical heat flux of water in pool boiling heat transfer," *Appl. Phys. Lett.*, vol. 83, no. 16, 2003.
- [3] H. Seon Ahn and M. Hwan Kim, "A Review on Critical Heat Flux Enhancement With Nanofluids and Surface Modification," *J. Heat Transfer*, vol. 134, no. 2, p. 024001, 2012.
- [4] S. D. Park, S. Won Lee, S. Kang, I. C. Bang, J. H. Kim, H. S. Shin, D. W. Lee, and D. Won Lee, "Effects of nanofluids containing graphene/graphene-oxide nanosheets on critical heat flux," *Appl. Phys. Lett.*, vol. 97, no. 2, pp. 3–5, 2010.
- [5] T. L. Bergman, F. P. Incropera, and A. S. Lavine, *Fundamentals of heat and mass transfer*. John Wiley & Sons, 2011.
- [6] S. Nukiyama, "The maximum and minimum values of the heat  $Q$  transmitted from metal to boiling water under atmospheric pressure," *Int. J. Heat Mass Transf.*, vol. 9, no. 12, pp. 1419–1433, 1966.
- [7] M. J. Allen, V. C. Tung, and R. B. Kaner, "Honeycomb carbon: a review of

- graphene,” *Chem. Rev.*, vol. 110, no. 1, pp. 132–145, 2009.
- [8] A. A. Balandin, S. Ghosh, W. Bao, I. Calizo, D. Teweldebrhan, F. Miao, and C. N. Lau, “Superior thermal conductivity of single-layer graphene,” *Nano Lett.*, vol. 8, no. 3, pp. 902–907, 2008.
- [9] J. Rafiee, M. A. Rafiee, Z.-Z. Yu, and N. Koratkar, “Superhydrophobic to superhydrophilic wetting control in graphene films,” *Adv. Mater.*, vol. 22, no. 19, pp. 2151–2154, 2010.
- [10] H. H. Cho, G. Choi, and D. Il Shim, “Can Graphene Lead to Breakthrough in Boiling Heat Transfer,” *J Mater. Sci Eng*, vol. 3, p. e109, 2014.
- [11] S. D. Park, S. W. Lee, S. Kang, S. M. Kim, and I. C. Bang, “Pool boiling CHF enhancement by graphene-oxide nanofluid under nuclear coolant chemical environments,” *Nucl. Eng. Des.*, vol. 252, no. 2012, pp. 184–191, 2012.
- [12] L. Zhang, Z. Yu, D. Li, L. Fan, Y. Zhu, R. Hong, Y. Hu, J. Fan, and K. Cen, “Enhanced Critical Heat Flux During Quenching of Extremely Dilute Aqueous Colloidal Suspensions With Graphene Oxide Nanosheets,” *J. Heat Transfer*, vol. 135, no. May 2013, p. 054502, 2013.
- [13] H. S. Ahn, J. M. Kim, and M. H. Kim, “Experimental study of the effect of a reduced graphene oxide coating on critical heat flux enhancement,” *Int. J. Heat Mass Transf.*, vol. 60, pp. 763–771, 2013.
- [14] S. W. Lee, K. M. Kim, and I. C. Bang, “Study on flow boiling critical heat flux enhancement of graphene oxide/water nanofluid,” *Int. J. Heat Mass*

- Transf.*, vol. 65, pp. 348–356, 2013.
- [15] H. S. Ahn, J. M. Kim, C. Park, J.-W. Jang, J. S. Lee, H. Kim, M. Kaviany, and M. H. Kim, “A novel role of three dimensional graphene foam to prevent heater failure during boiling,” *Sci. Rep.*, vol. 3, p. 1960, 2013.
- [16] J. M. Kim, T. Kim, J. Kim, M. H. Kim, and H. S. Ahn, “Effect of a graphene oxide coating layer on critical heat flux enhancement under pool boiling,” *Int. J. Heat Mass Transf.*, vol. 77, pp. 919–927, 2014.
- [17] S. Park, Y. Hwan, Y. Han, M. Taek, and N. Kim, “Journal of Industrial and Engineering Chemistry Effects of spray-deposited oxidized multi-wall carbon nanotubes and graphene on pool-boiling critical heat flux enhancement,” *J. Ind. Eng. Chem.*, vol. 24, pp. 276–283, 2014.
- [18] H. Seo, J. H. Chu, S.-Y. Kwon, and I. C. Bang, “Pool boiling CHF of reduced graphene oxide, graphene, and SiC-coated surfaces under highly wettable FC-72,” *Int. J. Heat Mass Transf.*, vol. 82, pp. 490–502, 2015.
- [19] P. Article, “The rise of graphene,” *Prog. Artic.*, pp. 183–191.
- [20] M. Segal, “Selling graphene by the ton,” *Nat. Nanotechnol.*, vol. 4, no. 10, pp. 612–614, 2009.
- [21] X. Lu, M. Yu, H. Huang, and R. S. Ruoff, “Tailoring graphite with the goal of achieving single sheets,” *Nanotechnology*, vol. 10, no. 3, p. 269, 1999.
- [22] Y. Zhang, J. P. Small, W. V. Pontius, and P. Kim, “Fabrication and Electric Field Dependent Transport Measurements of Mesoscopic Graphite Devices,”

- Appl. Phys. Lett.*, vol. 1, pp. 1–3, 2005.
- [23] A. K. Geim and K. S. Novoselov, “The rise of graphene,” *Nat Mater*, vol. 6, no. 3, pp. 183–191, Mar. 2007.
- [24] W. A. De Heer, C. Berger, X. Wu, P. N. First, E. H. Conrad, X. Li, T. Li, M. Sprinkle, J. Hass, M. L. Sadowski, and M. Potemski, “Epitaxial graphene,” *Solid State Commun.*, vol. 143, no. 1–2, pp. 92–100, 2007.
- [25] A. Reina, X. Jia, J. Ho, D. Nezich, H. Son, V. Bulovic, M. S. Dresselhaus, and J. Kong, “Large Area, Few-Layer Graphene Films on Arbitrary Substrates by Chemical Vapor Deposition,” *Nano Lett.*, vol. 9, no. 1, pp. 30–35, 2009.
- [26] D. A. Dikin, S. Stankovich, E. J. Zimney, R. D. Piner, G. H. B. Dommett, G. Evmenenko, S. T. Nguyen, and R. S. Ruoff, “Preparation and characterization of graphene oxide paper,” *Nature*, vol. 448, no. 7152, pp. 457–460, Jul. 2007.
- [27] W. S. H. Jr. and R. E. Offeman, “Preparation of Graphitic Oxide,” *J. Am. Chem. Soc.*, vol. 80, no. 6, p. 1339, 1958.
- [28] A. C. Ferrari, “Raman spectroscopy of graphene and graphite: disorder, electron--phonon coupling, doping and nonadiabatic effects,” *Solid State Commun.*, vol. 143, no. 1, pp. 47–57, 2007.
- [29] S. al Kline and F. McClintock, “Describing Uncertainties in Single-Sample Experiments,” *Eng*, vol. 75, pp. 3–8, 1953.
- [30] J. P. Hirth, G. M. Pound, and G. R. St. Pierre, “Bubble nucleation,” *Metall.*



- Trans.*, vol. 1, no. 4, pp. 939–945, 1970.
- [31] T. V. I. M. Anderson and I. Mudawar, “Microelectronic cooling by enhanced pool boiling of a dielectric fluorocarbon liquid,” *J. Heat Transfer*, vol. 111, no. 3, pp. 752–759, 1989.
- [32] A. E. Bergles and M. C. Chyu, “Characteristics of Nucleate Pool Boiling From Porous Metallic Coatings,” *J. Heat Transfer*, vol. 1, no. May 1982, pp. 279–285, 1982.
- [33] P. J. Marto, V. J. Lepere, M. Asme, and L. V. J. Lepere, “Pool boiling heat transfer from enhanced surfaces to dielectric fluids,” *J. Heat Transfer*, vol. 104, no. 2, pp. 292–299, 1982.
- [34] B. P. Athreya, R. L. Mahajan, and S. Sett, “Pool boiling of FC-72 over metal foams: effect of foam orientation and geometry,” in *Proc. of 8th AIAA/ASME Joint Thermophysics and Heat Transfer Conference, Jun, 2002*, pp. 24–26.
- [35] N. Zuber, “Hydrodynamic aspects of boiling heat transfer (thesis),” 1959.
- [36] S. J. Kim, I. C. Bang, J. Buongiorno, and L. W. Hu, “Effects of nanoparticle deposition on surface wettability influencing boiling heat transfer in nanofluids,” *Appl. Phys. Lett.*, vol. 89, no. 15, 2006.
- [37] H. M. Kurihara and J. E. Myers, “The effects of superheat and surface roughness on boiling coefficients,” *AIChE J.*, vol. 6, no. 1, pp. 83–91, 1960.
- [38] S. NISHIO and G. R. CHANDRATILLEKE, “Steady-state pool boiling heat transfer to saturated liquid helium at atmospheric pressure,” *JSME Int.*

- journal. Ser. 2, Fluids Eng. heat Transf. power, Combust. Thermophys. Prop.*, vol. 32, no. 4, pp. 639–645, 1989.
- [39] P. J. Berenson, “Experiments on pool-boiling heat transfer,” *Int. J. Heat Mass Transf.*, vol. 5, no. 10, pp. 985–999, 1962.
- [40] J. Y. Chang and S. M. You, “Enhanced Boiling Heat Transfer From Micro-Porous Cylindrical Surfaces in Saturated FC-87 and R-123,” *J. Heat Transfer*, vol. 119, no. 2, pp. 319–325, May 1997.
- [41] Y. V. Polezhaev and S. A. Kovalev, “Modelling heat transfer with boiling on porous structures,” *Therm. Eng.*, vol. 37, no. 12, pp. 617–621, 1990.
- [42] S. G. Liter and M. Kaviany, “Pool-boiling CHF enhancement by modulated porous-layer coating : theory and experiment,” vol. 44, pp. 4287–4311, 2001.
- [43] A. A. Watwe and A. Bar-Cohen, “Modeling of Conduction Effects on Pool Boiling Critical Heat Flux of Dielectric Liquids,” *ASME-PUBLICATIONS-HTD*, vol. 342, pp. 35–44, 1997.
- [44] M. Arik and A. Bar-cohen, “Effusivity-based correlation of surface property effects in pool boiling CHF of dielectric liquids,” vol. 46, no. 2003, pp. 3755–3764, 2006.
- [45] D. Xavier, S. Alvarez-garc, X. Diez-Betriu, S. Álvarez-García, C. Botas, P. Álvarez, J. Sánchez-Marcos, C. Prieto, R. Menéndez, and A. de Andrés, “Raman spectroscopy for the study of reduction mechanisms and optimization of conductivity in graphene oxide thin films,” *J. Mater. Chem.*

*C*, vol. 1, no. 41, pp. 6905–6912, 2013.